

On the attribution of weather events to climate change using a fit to extreme value distributions

Peter Sherman,^a Peter Huybers,^{a,b} and Eli Tziperman,^{a,b}

^a *School of Engineering and Applied Sciences, Harvard University, Cambridge, MA, USA*

^b *Department of Earth and Planetary Sciences, Harvard University, Cambridge, MA, USA*

arXiv:2308.07560v2 [physics.ao-ph] 28 May 2024

Corresponding author: Peter Sherman, petersherman@g.harvard.edu

ABSTRACT: Increases in extreme weather events are a potentially important consequence of anthropogenic climate change (ACC), yet, are difficult to attribute to ACC because the record length is often similar to, or shorter than, extreme-event return periods. This study is motivated by the “World Weather Attribution Project” (WWA) and, specifically, their approach of fitting extreme value distribution functions to local observations. The approach calculates the dependence of distribution parameters on global mean surface temperature (GMST) and uses this dependence to attribute extreme events to ACC. Applying this method to preindustrial climate simulations with no time-varying greenhouse gas forcing, we still find a strong dependence of distribution parameters on GMST. This dependence results from internal climate variability (e.g., ENSO) affecting both extreme events and GMST. Therefore, dependence on GMST does not necessarily imply an effect of ACC on extremes. For three different cases examined by WWA we find that the parametric relationship between weather and GMST is indistinguishable between simulations that are and are not forced by greenhouse gasses. We further consider for these three cases whether an extreme value, normal, or log-normal distribution better represents the data; if a GMST-dependence of distribution parameters is justified using a likelihood ratio test; and if a meaningful attribution is possible given uncertainties in GMST dependence. In one case we find that an attribution of Australia’s 2020–2021 Bushfires to ACC is difficult due to the effects of Natural variability. In another involving the 2019–2021 drought in Madagascar we find that the small number of available data points precludes a meaningful attribution analysis. Overall, we find that the effects of natural climate variability on GMST and the uncertain relationship between GMST and regional extremes may lead to inaccurate attribution conclusions using the WWA approach.

1. Introduction

The Intergovernmental Panel on Climate Change (Core Writing Team et al. 2023) found that global mean surface temperature (GMST) between 2011–2020 was 1.09°C [0.95 °C–1.20°C] above preindustrial levels. Although climate change is clearly manifested in GMST warming, and there are reasons to expect extreme events to change with mean climate, it is a complex task to attribute individual extreme weather events to anthropogenic climate change. Extreme events—including heatwaves, droughts, and floods—are rare by definition, so the observational record may be too short to detect anthropogenic signals. This issue is especially pervasive in lower-income countries where data are sparse and the historical record is short (Otto et al. 2020). The situation is further problematic for extreme precipitation event attribution, which is highly sensitive to the specific timescales and percentiles used to define extreme precipitation events (Pendergrass 2018).

The field of attribution of extreme events has progressed significantly over the past decade and encompasses several approaches (see example reviews and cited references within, Stott et al. 2010; Hegerl and Zwiers 2011; National Academies of Sciences 2016; Clarke et al. 2022; Philip et al. 2020). The approaches that have been applied include the fraction of attributable risk (FAR, Allen 2003; Stott et al. 2004), using simulations from climate models, using constraints derived from optimal fingerprinting techniques (Christidis et al. 2015), using climate models to validate observed probability density functions (PDFs) (Perkins et al. 2007), and the “Analogue-Based Approach” (Lorenz 1969; Yiou et al. 2007; Vautard and Yiou 2009; Faranda et al. 2022). Another methodology fits statistical distributions to the historical record (again, either observed or from climate models) in what Stott et al. (2016) refer to as “Empirical-Based Approaches.” This approach assesses how the return period of particular events has changed over the historical record, with the purpose of detecting potential trends in the frequency of extreme events. These statistical approaches have been used to study trends in extreme events such as flooding in Thailand in 2011 (Van Oldenborgh et al. 2012). Stott et al. (2016) note that approaches using climate models allow for a better estimate of the magnitude and direction of the human-induced contributions to an extreme event than is possible using observations alone.

Another use of climate models is based on single-model initial condition large ensembles (LE), composed of a climate model run several times with slightly different initial conditions. Averaging over multiple climate model ensemble members can reduce the signal of internal variability,

facilitating the identification of forced climate change signals. This averaging generally improves the detection of trends in the magnitude or frequency of an extreme event, which are difficult to quantify in a single simulation or in the observational record where the signal from internal variability may be dominant (Yoshida et al. 2017; Yamaguchi et al. 2020). These simulations have been used in the context of tropical cyclone slowdown (Yamaguchi et al. 2020), as well as drought events in South and East Africa (Lott et al. 2013; Pascale et al. 2020). The detection and attribution literature is extensive, and for a further detailed discussion, we refer the reader to the above reviews and to recent studies (Stott et al. 2016; Knutson et al. 2017; Seneviratne et al. 2021).

One particular approach that is the focus of this paper and that has been used in recent years as a rapid response to extreme events attempts to fit the observed data to an extreme value PDF. The fit allows for a dependence of the distribution parameters on explanatory variables, typically the GMST (e.g., Ciavarella et al. 2021; van Oldenborgh et al. 2021; Harrington et al. 2022; Philip et al. 2020). A GMST dependence is then interpreted as a response of extreme events to anthropogenic global warming. This dependence is then used to attribute extreme events by quantifying the effects of anthropogenic forcing on the probability of their occurrence. Technically this is achieved by writing the location parameter of the extreme event distribution, μ , as a function of \bar{T} , the (low-pass filtered, via a 4-year running average) GMST “as a measure of anthropogenic climate change” (Harrington et al. 2022), such that $\mu = \mu_0 + \alpha \bar{T}$. The GMST-dependence, α , is estimated via a fit to observations. The fitted PDF is then used to evaluate the probability of extreme events at 1900, $P(\mu_0 + \alpha \bar{T}(1900))$ relative to those at 2020, $P(\mu_0 + \alpha \bar{T}(2020))$. This allows for estimating how the probability of an extreme event changed between these times. This approach has been used by the World Weather Attribution Project (WWA, <https://www.worldweatherattribution.org/>). Whereas our focus is on this observational approach to attribution, it should be noted that WWA also makes use of climate model simulations in interpreting extreme events.

Motivated by these pioneering efforts based on the fit to extreme event PDFs, we re-examine three test cases analyzed by WWA: the Siberian Heatwave analysis of Ciavarella et al. (2021, hereafter CC2021), the analysis of high temperatures associated with the Australian Bushfire by van Oldenborgh et al. (2021, hereafter OK2021), and the Madagascar Drought analysis of Harrington et al. (2022, hereafter HW2022). These cases were chosen as they represent a range of applications, including the attribution of heatwaves at high and low latitudes (Siberia vs. Australia)

and of a drought extreme. Each of these studies leverages either a Generalized Extreme Value (GEV) or Generalized Pareto Distribution (GPD) fit to assess potential contributions to extreme events from anthropogenic climate change. WWA studies use both climate model simulations and observational analysis, and we focus on the observational component. In each of the three cases we use the CESM Large Ensemble (Kay et al. 2015) to put the observed instrumental record into perspective, and we explore potential caveats concerning the methods examined and suggest how these limitations might be addressed.

An important issue to address before getting into the technicalities is the formulation of the null hypothesis in an attribution study that uses GMST-dependent distribution parameters to deduce the effects of anthropogenic climate change. The effects of anthropogenic climate change on extreme events are parameterized by the term α in WWA studies, $P(\mu_0 + \alpha \bar{T})$. Although WWA does not provide a detailed discussion of the null hypothesis that they assume in the absence of anthropogenic climate change, the implied null hypothesis is that α is zero (see Section 4.3.1 of Philip et al. 2020).

We find here that in a preindustrial climate model run, the fit of Australian heat extremes leads to values of α that are substantially greater than zero in the absence of anthropogenic climate change because of the effects of natural climate variability (by which we mean internal variability due to modes such as ENSO as opposed to volcanic-driven natural variability). Our findings thus show that the null hypothesis can be rejected even in the absence of anthropogenic climate change, complicating the WWA approach. The issue related to the null hypothesis that our analysis exposes is simple: natural variability modes such as ENSO affect both local temperature extremes and the GMST. In some cases, the effect on local extremes (say the effects of ENSO on heatwaves in Australia) may be large, but the effect on GMST is small. This might lead to the false conclusion that a small GMST signal leads to a comparatively large effect on local extremes.

Our study addresses four questions: (1) Is a GMST dependence of the PDF parameters necessarily an indication of the signal of anthropogenic climate change? (2) Is a GEV or GPD necessary to fit the available observations, or is a more standard distribution (normal/log-normal) sufficient? (3) Is the addition of GMST-dependent distribution parameters, which form the basis for the attribution analysis, justified statistically, and is the error level (the uncertainty range of α) in this dependence sufficiently small to allow for attribution? (4) What do Single-Model Initial-Condition Large

Ensembles tell us about the amount of data needed to determine the GMST dependence with confidence?

We note that WWA uses multiple attribution tools, including model runs and the analysis of observations (Philip et al. 2020). Similarly, WWA often uses multiple climate models and is careful to exclude models based on their performance and return periods relative to the observed one (e.g., Pinto et al. 2023), whereas we use a single model (CESM) to demonstrate some of our points and focus on observational analysis. We focus on one aspect only of this richer approach, involving a fit of observations to extreme value distributions. Additionally, our goal is limited to evaluating the observational approach and suggesting additional tests to examine its robustness rather than coming up with alternative attribution approaches.

The rest of the paper is structured as follows. Section 2 describes the statistical models, observation datasets, and methodologies. Section 3a shows that a GMST-dependence of distribution parameters does not necessarily represent the effects of anthropogenic climate change using an analysis of a CESM preindustrial simulation (i.e., without time-varying anthropogenic and natural forcings). We then further examine the three attribution cases in the remainder of section 3. Section 4 provides a summary and discussion of the results.

2. Methods and Data

In this section, we briefly describe the extreme value distributions used in the following sections (a and b) and discuss uncertainty estimates and empirical cumulative distribution functions (CDFs) that we will use later (c). We describe the deviance statistic test which we use to examine the justification for adding GMST-dependent parameters (d), and the mean residual life plot used to test the justification for using a GPD and its threshold value (e). The data used are described in section (f).

a. The Generalized Extreme Value (GEV) distribution

Extreme value distributions are a family of PDFs that can be used to represent the statistical behavior of block maxima or minima of a record. An example is an annual time series of the maximum daily temperature at each year, the “block” being one year in this case. It can be shown that the distribution of such maxima follows one of three classes of PDFs: Gumbel, Fréchet, or

Weibull (Coles et al. 2001), depending on the shape of the tail of the distribution of the events for which block maxima are calculated. Rather than explicitly specifying one of these three classes in fitting extreme data, one can combine these distributions into one functional form, represented by the Generalized Extreme Value (GEV) distribution. Large quantities of data are typically needed to accurately fit a GEV and calculate its parameters (e.g., Philip et al. 2020; Trevino et al. 2020).

The PDF of a variable x whose statistics are governed by the GEV is given by

$$GEV(x, \mu, \sigma, \xi) = \frac{1}{\sigma} t(x, \mu, \sigma, \xi)^{\xi+1} e^{-t(x, \mu, \sigma, \xi)}, \quad (1)$$

where

$$t(x, \mu, \sigma, \xi) = \left(1 + \xi \frac{x - \mu}{\sigma}\right)^{-1/\xi}, \quad (2)$$

under the assumption that $\xi \neq 0$. If $\xi = 0$, $t(x, \mu, \sigma, \xi)$ is defined as,

$$t(x, \mu, \sigma, \xi) = e^{-\frac{x - \mu}{\sigma}}. \quad (3)$$

In some of the attribution studies we follow for this paper (specifically, CC2021 and OK2021), the location parameter μ is assumed to vary linearly with the 4-year smoothed GMST \bar{T} , as,

$$\mu = \mu_0 + \alpha \bar{T}. \quad (4)$$

Estimation of the parameter α is the key to the attribution of extreme events. However, this determination may be limited due to the short observational record (Zwiers et al. 2011; De Paola et al. 2018). To estimate the mean μ_0 , scale parameter σ , the GMST dependence α , and the shape parameter ξ , we follow Coles et al. (2001) and WWA (Philip et al. 2020) and maximize the log-likelihood of the data points x_t using a GEV distribution,

$$l(\mu_0, \sigma, \xi, \alpha) = \sum_{t=1}^m \log(GEV(x_t, \mu_0, \sigma, \xi, \alpha)). \quad (5)$$

We apply this approach, following CC2021 and OK2021, to observations and to data from the CESM Large Ensemble (Kay et al. 2015).

b. Generalized Pareto Distribution (GPD)

In some applications, one is interested only in points in a time series that exceed a specified threshold, whose statistics are represented by the Generalized Pareto Distribution (Coles et al. 2001). In order to study the extreme drought events in Madagascar using a record of precipitation, HW2022 fit a Generalized Pareto Distribution (GPD) to the bottom 20th percentile of precipitation, i.e., years associated with drought. This low tail was converted to a high tail by multiplying the precipitation data by -1 . Although this converts the lowest precipitation values to maxima, the transformed data have a hard maximum at zero. We note that the validity of using a GPD, in this case, is questionable because no such hard maximum is allowed by—or represented in the functional form of—the GPD.

The PDF of the GPD is given by

$$GPD(x, \mu, \sigma, \xi) = \frac{1}{\sigma} \left(1 + \xi \frac{x - \mu}{\sigma} \right)^{-\left(\frac{1}{\xi} + 1\right)}. \quad (6)$$

HW2022 assumed that the threshold parameter, which they denote μ (denoted u by Coles et al. 2001) and scale parameter σ both depend exponentially on the 4-year running-averaged GMST, \bar{T} such that,

$$\begin{aligned} \mu &= \mu_0 \exp(\alpha \bar{T} / \mu_0), \\ \sigma &= \sigma_0 \exp(\alpha \bar{T} / \mu_0). \end{aligned} \quad (7)$$

The exponential fit was assumed by HW2022 in order to ensure that the scaling factor $\exp(\alpha \bar{T} / \mu_0)$ applied to both μ_0 and σ_0 is strictly positive, so the distribution has fixed dispersion. We obtain the optimized GPD parameters $(\mu_0, \sigma, \xi, \alpha)$ by again maximizing the log-likelihood (Eq. 4.10, Coles et al. 2001),

$$l(\mu, \sigma, \xi) = \sum_{t=1}^m \log(GPD(x_t, \mu, \sigma, \xi)), \quad (8)$$

using the trust-region constrained algorithm in the Scipy minimize Python package ('trust-constr' method).

The GPD requires the bound $\sigma > 0$ and consistency relations of the form $x \geq \mu$ (for $\xi \geq 0$), and $\mu \leq x$ and $x \leq \mu - \sigma / \xi$ (for $\xi < 0$). As the optimization iteratively attempts to search for the optimal

parameter values, these constraints are occasionally violated, leading to complex numbers or NaNs (not a number) in the likelihood. The GPD optimization is notably more prone to such failures and sensitive to the initial guesses of $\alpha, \mu_0, \xi, \sigma$ than the GEV optimization. In order to avoid such search failures, we replace complex and NaN terms in the log-likelihood sum with large penalty terms whenever they occur due to constraints being violated. In addition, if the optimization fails, we re-run the optimization again with new randomly selected initial guesses until convergence to a solution that maximizes log-likelihood and that satisfies the constraints occurs. We note that related solutions have been used to deal with GEV/GPD convergence issues by Robin and Ribes (2020).

c. Uncertainty estimates and empirical cumulative distribution functions

We follow WWA studies and use non-parametric bootstrapping to estimate uncertainty ranges for the optimized parameters. In particular, we use the uncertainty in α as one way to evaluate the validity of the attribution results. We also compare the appropriately fitted distributions (GEV and normal distributions for extreme temperatures or GPD and log-normal for droughts) to the empirical cumulative distribution functions (CDFs) of the observations to assess the quality of the fit. The empirical CDF is calculated by sorting extreme values (either temperature or precipitation) from smallest to largest, calculating the cumulative sum, and normalizing to a maximum CDF value of one. We calculate error bars in the empirical CDFs based on bootstrap resampling with replacement of the observations. The empirical CDF is calculated for each sampling, and we then calculate the 90th and 95th percentiles from the resulting distribution at each value of the variable whose CDF is estimated. In order to estimate uncertainty in the parameters estimated from our GEV or GPD maximum likelihood fit, we similarly use bootstrap resampling. We sample with replacement the GMST and corresponding extreme temperature record 5,000 times and optimize the parameters for each resampling. We then estimate the 90th and 95th percentiles from 5,000 bootstrap samples. For the Madagascar precipitation case, we perform 5,000 bootstrap resamples when analyzing the observations, but 1,000 bootstrap resamples when analyzing the CESM Large Ensemble due to the slow convergence and expensive computations using the GPD log-likelihood maximization.

d. Deviance Statistics (Likelihood Ratio Test)

In general, when fitting a model to data, if the number of fit parameters is increased, one expects a better fit because of the greater flexibility of the fitted model. Specifically, in the case considered here, adding a parameter α to include the GMST dependence of the location/threshold parameter will increase the maximum log-likelihood of the data. The salient question is whether the improvement in the fit exceeds that expected simply on account of the larger number of model parameters. To evaluate the improvement of the fit, Coles et al. (2001, theorem 2.7) recommend the use of a deviance statistic, also known as a likelihood ratio test. This test uses a measure, D , equal to twice the difference of the sum of log-likelihoods of the model with k additional parameters minus that of the simpler model. Because more parameters lead to a better fit and thus higher log-likelihood, D is non-negative. D is then compared to a χ_k^2 distribution to assess if the k additional parameters significantly improve the likelihood. For example, with $k = 1$, the 95th percentile of χ_1^2 is equal to 3.8. If D is larger than this threshold, we conclude that adding an additional parameter significantly improved the fit. It can then be inferred that the added parameter—in our specific case, the GMST dependence, α —meaningfully explains features of the data. On the other hand, if the deviance statistic is not significant, one concludes that the addition of another parameter to the statistical fit is not justified by the data and, therefore, that this parameter cannot be used to draw conclusions about the data. Specifically, if one finds that the addition of α is not justified, the implication is that the estimated value should not be used to calculate the effects of climate change on the extreme events under examination. We also estimate the distribution and uncertainty of D through bootstrap resampling of the data 5,000 times.

e. Mean residual life plot

In the process of fitting a GPD, a minimum threshold is chosen to select the data that represent extreme values that should be fit. The GPD fit can be sensitive to the selection of this threshold, where too low of a threshold could violate the asymptotic nature of the GPD, and too high of a threshold would provide only a few relevant data points and lead to an unstable fit. In order to determine an appropriate threshold, one leverages what is known as the mean residual life (MRL) plot. The MRL uses the GPD-based expectation value of the data (Eq. 4.8, Coles et al. 2001). For a given threshold, u_0 , the expectation value (mean) of the data X that exceed the threshold can be

written for $\xi < 1$ as,

$$E(X - u_0 | X > u_0) = \frac{\sigma_{u_0}}{1 - \xi}.$$

It can be shown that for all thresholds $u > u_0$, this expectation value is (Eq. 4.9, Coles et al. 2001),

$$E(X - u | X > u) = \frac{\sigma_{u_0} + u\xi}{1 - \xi}. \quad (9)$$

That is, for $u > u_0$, $E(X - u | X > u)$ is a linear function of u . This expected linearity of Equation 9 with u —for values of u for which the GPD fit is appropriate—can be used to test the validity of the chosen threshold used in the GPD analysis via a plot which we use in our results section known as the MRL plot.

f. Data

We briefly review the observations and our processing used in each of the three case studies re-considered here. In addition, we describe the model Large Ensemble and preindustrial simulations that we analyze.

(i) Siberian Heatwave. Following CC2021, we rely on two sets of observations: (1) daily maximum temperature extremes for each year from station data in Verkhoyansk as discussed in CC2021; and (2) 4-year smoothed GMST anomalies from GISTEMP (Lenssen et al. 2019). CC2021 also performed a GEV analysis on temperature anomalies over a region in Siberia, which we do not focus on here in order to study specifically the extreme values detected at the Verkhoyansk station. At the time of the CC2021 study, the daily maximum temperature extreme in 2020 at the Verkhoyansk station was recorded as 38°C. This temperature extreme currently appears as a missing data point on the National Climatic Data Center website (<https://www.ncdc.noaa.gov/cdo-web/search>, station RSM00024266, VERHOJANSK, data downloaded Aug 2023) but we still use this unconfirmed value in our analysis. We also study GMST anomalies and extreme temperatures over the Siberian region defined in CC2021 within the CESM Large Ensemble (Kay et al. 2015) over the period 1926–2019. The CESM Large Ensemble contains 42 simulations of the climate over the period 1920–2100 under historical and RCP 8.5 external forcing, of which we use the 35 that were run on the NCAR supercomputer. We use model output only up to the year 2020, and as a result, there should be little sensitivity to the emissions scenario used (DAMIP, Gillett et al. 2016, uses RCP

4.5), as the emissions scenarios begin to significantly diverge only later. These simulations differ only in small perturbations to the initial conditions, which lead to different temporal sequences of internal variability. Similarly, we study analogous variables within a 1,800-year CESM preindustrial simulation, yielding 18 segments of 94 years for consistency with the length of the observed record.

(ii) *Australian Bushfire.* Following OK2021, we again use two sets of observations for the years 1920–2019: (1) annual (July–June) maxima of 7-day moving average daily-maximum surface temperature data from the Australian Water Availability Project (AWAP) over a region in Australia defined in OK2021; and (2) 4-year smoothed GMST anomalies from GISTEMP. We again apply the same analysis to the CESM Large Ensemble and to the long CESM preindustrial run, in this case using 18 segments of 98 years, for consistency with the observations.

(iii) *Madagascar Drought.* Following HW2022, we used two datasets. (1) 2-year means of precipitation from ERA5 (Hersbach et al. 2020) over the region of Madagascar that was defined in HW2022. HW2022 explained that they used a “24-month running mean rainfall data from July to June.” Our approach is to calculate total annual precipitation and then calculate a running 2-year average of this annual data resulting in a new smoothed annual time series. For 1951–2020 the bottom 20% precipitation 2-year periods are selected for the analysis, corresponding to the following 14 two-year periods: 1956–1957, 1957–1958, 1958–1959, 1959–1960, 1962–1963, 1990–1991, 1991–1992, 1992–1993, 2008–2009, 2009–2010, 2015–2016, 2016–2017, 2017–2018, 2019–2020. (2) 4-year smoothed GMST anomalies from GISTEMP. We note that the analysis following HW2022 relies on a fit to only 14 data points. We discuss the issues that are involved in fitting extreme distribution functions to such a small number of data points below. We also study the equivalent variables within the CESM Large Ensemble over the period 1950–2019, consistent with the period of observations. We again apply the same analysis to the CESM Large Ensemble and to the long CESM preindustrial run, in this case using 18 segments of 70 years.

WWA uses two variants of their analysis approach, one in which the extreme data point being attributed is incorporated into the estimate of the PDFs and one in which it is not (Philip et al. 2020). We chose to use the second approach. Inclusion of the extreme being analyzed in the calculation will tend to make the parametric dependence on GMST larger, and tend to make it easier to reject the null of no change in favor of the alternate hypothesis. In the present case, we

are still unable to reject the null hypothesis, such that the exclusion of the event in question will not change the result.

We note that in each of these three case studies, WWA leverages many datasets, including ERA5 reanalysis, station observations, and the multimodel CMIP5 ensemble. We use only a subset of the data they study and also the CESM Large Ensemble data for self-consistency in comparing the three examples that we analyze here.

3. Results

Our analysis of the attribution of extreme events based on a fit to extreme value distributions is presented as follows. First, in subsection 3a, we assess the null hypothesis that a lack of influence of anthropogenic climate change should result in no GMST dependence of the distribution parameters or in α being indistinguishable from zero. We do so by analyzing a 1,800-year CESM preindustrial simulation. The preindustrial simulation uses fixed greenhouse gas concentrations, volcanic activity, anthropogenic aerosols, land use, and solar forcing all set to their respective levels in the year 1850. Most importantly in the context of this study is the lack of a time-varying anthropogenic greenhouse gas forcing in this simulation. In the following three sections (3b, 3c, 3d) we then consider each of the three test cases and first assess the need for a GMST dependence and also for using a GEV or GPD fit to the observations as opposed to that of a normal or log-normal distribution. We then evaluate whether there is a statistically significant GMST dependence using the deviance statistic. Finally, we estimate the uncertainty level of the parameter α used for the attribution and evaluate the GEV or GPD fit to the CESM Large Ensemble in order to deduce the amount of data needed to adequately constrain GMST dependence.

a. Extremes analysis of a pre-industrial simulation

WWA examines the dependence of the distribution parameters of extreme events on the (4-year running mean) GMST and, if α is significantly greater than zero, to infer that anthropogenic climate change affects these extreme events. Furthermore, the parameter α representing the dependency on GMST is then used to quantify how much a given extreme event was made more likely as a consequence of climate change. We show here that it is possible, however, for internal climate variability, such as ENSO, to produce covariance between GMST and extremes even

without anthropogenic influences. This is demonstrated most clearly in this section by using a pre-industrial climate model run, and we further elaborate using the CESM Large Ensemble as well. More importantly, for attribution purposes, this would suggest that the value of α calculated in the presence of a GHG increase can be affected by natural variability, biasing the attribution results.

To examine this potential role of internal variability, we start with the case of the hot weather associated with the Australian Bushfires and perform a GEV analysis using a 1,800-year CESM preindustrial run. This run is done without time-varying changes to anthropogenic CO₂, other anthropogenic greenhouse emissions, volcanic (natural) emissions, land use changes, or aerosols. These are all held constant at year 1850 values. We use 18 data segments of length 94 years, equal to the length of the observed record and analogous to having 18 simulations of historical climate with no changing anthropogenic emissions. The distribution of α values for the GEV preindustrial analysis are shown by the green bars in Fig. 1a. Despite no increase to anthropogenic forcing being applied to the preindustrial run, we find a large and positive α calculated from essentially all model output segments centered around a median value of 4.9 °C per °C. The large α value means that for every 1 °C GMST warming, extreme summer temperatures increase by 4.9 °C. Note that, following WWA, we are using four-year-running average GMST values for this computation.

It is difficult to imagine a physical causal mechanism that would lead to such an enormous amplification of the GMST signal in Australian heatwaves. Instead, internal variability, for example ENSO, could increase both extreme temperatures over Australia and, to a much smaller degree, affect GMST, creating this seemingly strong dependence between extreme events and GMST. It is known that several modes of internal variability affect extreme temperatures in Australia, including ENSO, the Indian Ocean Dipole, and the Southern Annular Mode (Hendon et al. 2007; Ummenhofer et al. 2009; King et al. 2020). The covariance between this extreme and GMST found in the CESM Large Ensemble analysis thus must result from another factor (internal climate variability, such as ENSO) affecting both Australian temperatures and global mean temperatures. This highlights a potential major difficulty with analyses based on a fit of distribution parameters to GMST. When analyzing the observed record in section c below, we find $\alpha \approx 2$ °C per °C. This suggests a two-degree warming of extreme events for a one-degree warming of the GMST. Given

the results here, it is more likely, however, that this estimate for α is influenced by natural variability as demonstrated by analyzing the preindustrial run with a time-invariant anthropogenic forcing.

The same analysis for Siberian heatwaves (green bars in Fig. 1b) shows that the value for α deduced from a record of a similar length to that of the observations' ranges between 1 to 4, although there is again no time-varying anthropogenic forcing in the corresponding model run. This large and variable response shows that a non-zero α does not necessarily imply an effect of anthropogenic climate change. The base hypothesis that a non-zero GMST dependence implies an anthropogenic signal is contradicted by the above analysis.

For the Madagascar Drought example (Fig. 1c), we find a large spread in both the preindustrial run as well as the CESM Large Ensemble, centered around zero in both cases. The fact that the α distribution from the preindustrial run is centered around zero suggests that a null hypothesis of $\alpha = 0$ could be appropriate in this case. That is, low extremes of precipitation show no significant increase or decrease related to GMST in either the forced or unforced runs. We further consider this case below using observations.

The results for Australian extremes (Figs. 1a) show that the distribution of α in increasing GHG forced simulations (blue bars) is closer to zero than in the unforced simulations (green bars). This demonstrates that α is affected by both GMST and by the weak projection of regional natural variability on the GMST. In the first case, a sensible null hypothesis is that the PDF of heat extremes is shifted by the warming in GMST as may be better represented by $\alpha = 1$, while we saw that the second case can lead to large α values. In simulations with time-varying anthropogenic forcing, there is no way to tell what the effect of natural variability on α is using this approach, so the magnitude of α appears a poor indicator of anthropogenic influence.

WWA recognizes that α may be strongly affected by natural variability and uses the 4-year running mean GMST to filter out the effects of natural variability. The analysis in this paper, however, shows that this approach is insufficient and that such variability can still lead to a large α even with smoothing. We conclude that in a more typical scenario analyzed using the WWA methodology and applied to observations under varying GHG, the value of α may still be affected by natural variability and, therefore, may bias the estimates of the effect of anthropogenic climate change on the return time of extreme events. One could justify the WWA use of the 4-year averaged GMST as being a proxy for known greenhouse gas concentrations. If CO_2 were indeed used, the

analysis of the preindustrial run, would, of course, lead to $\alpha = 0$, eliminating this problem. But WWA studies use GMST and we follow that methodology here.

The result that natural variability may strongly affect α when the 4-year average GMST is used to link extreme events to anthropogenic climate change suggests that it might be useful to reevaluate some of the WWA results based on the fit to extreme distributions in at least the three studies that we review. It is possible, of course, that a strong anthropogenic signal in a few decades could significantly affect extreme events and overwhelm the effects of natural variability in cases such as the Siberian Heatwave. The attribution of extreme temperatures would be more difficult in cases like the Australian example, where the effects of natural variability are large, as indicated by the large α detected in the CESM preindustrial simulation. In such cases, it would be important to correctly identify all relevant covariates (such as ENSO in the Australian case) and note that misleading results for α may be obtained if one relies only on GMST. It is, therefore, necessary to study when and how such an emergence of the ACC signal out of natural variability occurs for this attribution analysis to be used with confidence. We next proceed to consider other uncertainties involved in the attribution analysis based on a fit of extreme value distributions.

b. Siberian Heatwave

We now explore other facets of the attribution of the Siberian Heatwave in the summer of 2020 to anthropogenic change, notwithstanding the foregoing finding that the interpretation of α is complicated by the presence of natural variability. We focus specifically on the CC2021 analysis of the June daily maximum temperatures because it allows us to address the question of whether the data justify the use of non-stationary (GMST-dependent) extreme value distributions.

While it is understood based on theoretical considerations that a GEV is the appropriate representation of block-maxima of data (Coles et al. 2001), it is not obvious for a given problem what minimum block size justifies using a GEV, and specifically if a year of daily maximum data suffices. This is especially an issue given that the temperature is auto-correlated and, therefore, more data are needed per averaging block to justify the use of a GEV. It is, therefore, worthwhile to check how well a more standard (say normal) distribution performs in fitting the data.

A cumulative distribution estimate of the highest June daily-maximum temperature observed each year between 1926–2020 at the Verkhoyansk station is shown in Fig. 2a along with a 95%

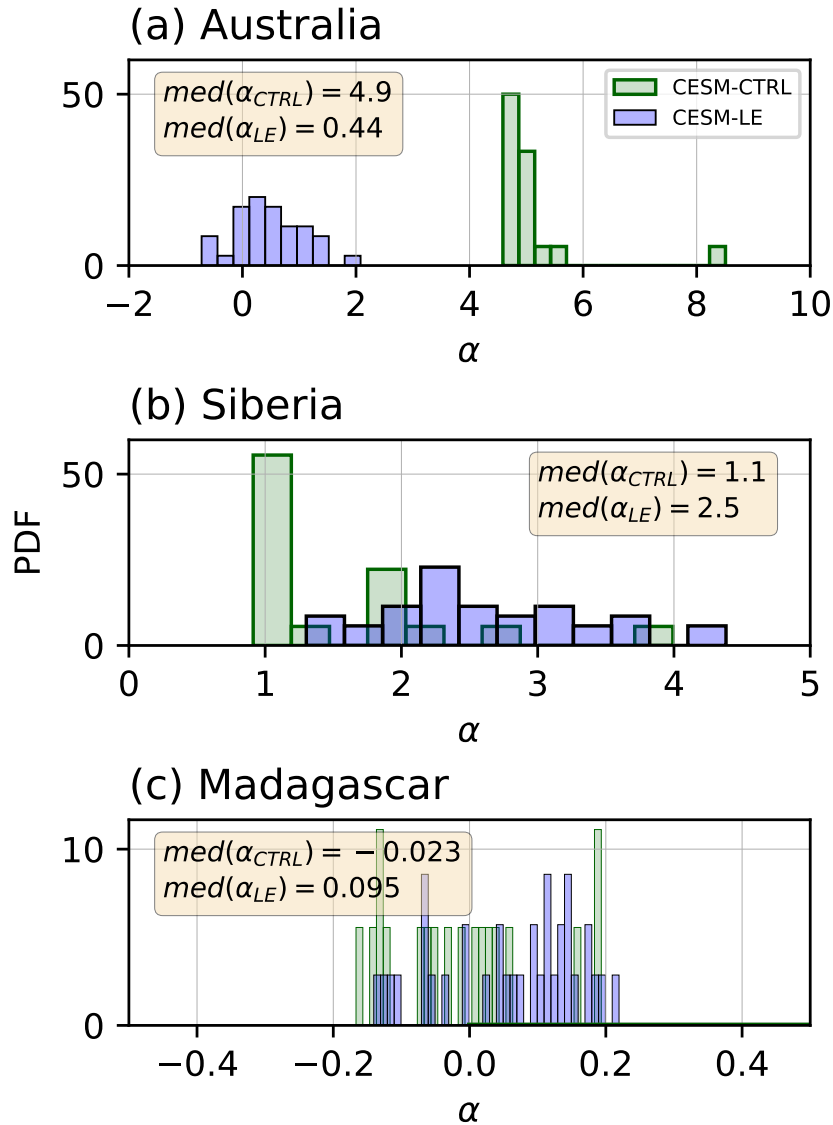


FIG. 1. **Effect of natural climate variability on α distribution.** PDFs of α for (a) The Australian 7-day moving mean of the maximum temperature related to the analysis of the 2019–2020 bushfires. (b) The Siberian maximum daily temperatures that were used in the analysis of the 2020 heatwave. (c) The Madagascar 2-year precipitation used in the analysis of the drought of 2019–2021. The analyses are based on the 1,800-year CESM preindustrial run with 94-, 98-, and 70-year segments, respectively (green), and the 35 Large Ensemble members (blue). The lengths of these segments correspond to the extent of the observed records used in CC2021, OK2021, and HW2022. The median values for the CESM preindustrial and Large Ensemble for each of the cases are indicated in the boxes. The median values are Australia: $\alpha_{CTRL} = 4.9$, $\alpha_{LE} = 0.4$; Siberia: $\alpha_{CTRL} = 1.1$, $\alpha_{LE} = 2.5$; Madagascar: $\alpha_{CTRL} = -0.02$, $\alpha_{LE} = 0.09$.

confidence interval of the CDF obtained by bootstrapping. In the first step of our analysis, we consider cumulative distribution function fits to the observed distribution, assuming the data follows either a GEV or normal distribution. The fitted distributions are specified here to be stationary (by setting $\alpha = 0$ and $\mu = \mu_0$ in Eqns. 1–4). Fits are obtained by maximizing the likelihood of the data, and the results are shown in Fig. 2a. Both distributions generally fit the observations well, with the normal fit completely within the 95% range of the observed distribution, and with the GEV fit being good except at the highest temperature, where it slightly underestimates the probability of obtaining the highest temperatures. There is only one data point above 35 °C, so the empirical CDF is poorly constrained there in any case. Interestingly, the normal distribution and GEV CDFs look similar and lie within the confidence intervals defined for the empirical CDF, despite the normal distribution having fewer parameters than the GEV. It is worth noting that a GEV and a normal distribution may assign very different probabilities to extreme events even when the two distributions provide an adequate fit to the observed CDF.

The quality of fits seems to suggest that an extreme value distribution may not be needed as a normal distribution does just as well. Similarly, a non-stationary distribution with $\alpha \neq 0$ may not be necessary given that the stationary distributions seem to provide a satisfactory fit to the empirical cumulative distributions, and we further examine this next. While CDFs are commonly used to differentiate between distribution functions, as in the Kolmogorov-Smirnov test, plots of the PDFs (Supplementary Fig. SI-1) for the three distributions (normal, GEV and empirical) also suggest that the normal distribution aligns well with the observed data (and mostly that the data may not be sufficient to well-constrain the distribution). An application of Occam’s razor principle would, therefore, suggest that the simpler Gaussian distribution should be used rather than a GEV if there is not a significant improvement in the distribution fit with the GEV. This is also discussed by Philip et al. (2020) who mention explicitly that the extreme value distributions may not outperform a simpler (Gaussian) distribution in some cases. Otto et al. (2018) concluded that a Gaussian distribution is justified because the events in question are not very rare. CC2021 found that a Gaussian distribution fits the data well but proceeded to use a GEV for the bulk of the analysis. These results all question the need for extreme value distribution functions when it comes to attribution analysis.

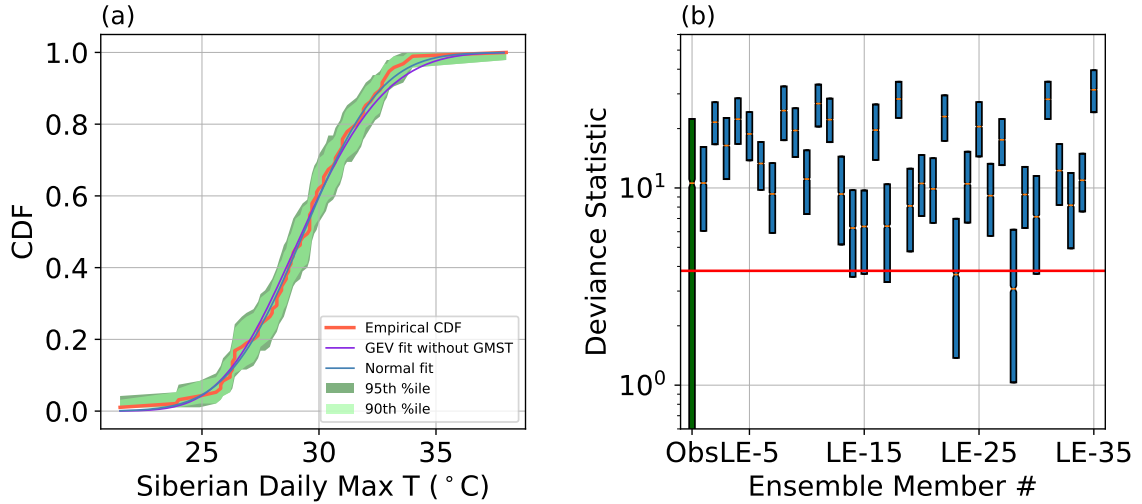


FIG. 2. **Siberian Heatwave: (a) Testing the need for a GEV fit.** The red curve indicates the empirical CDF of the highest daily maximum temperature for each year for the Verkhoyansk station data. The purple and blue lines denote fits by a GEV (with a constant location parameter) and by a normal distribution, respectively. The light and dark green shadings correspond to 90th and 95th percentile confidence intervals (section 2c). **(b) Justification for using a GMST-dependent mean.** Box plots of the deviance statistic between a GEV distribution without a GMST-dependent mean relative to a GEV distribution with a GMST-dependent mean using the Siberian heatwave data with 5,000 bootstrap resamples. The edges of the boxes correspond to the first and third quartiles. The deviance statistic for the station observations is shown in green as the leftmost box. The deviance statistic was also computed for each of the 35 members from the CESM Large Ensemble (blue). The 95th percentile significance level from a $\chi^2_{k=1}$ distribution with one degree of freedom is shown by the horizontal red line, corresponding to the addition of one degree of freedom by including α in the fitted model.

We now proceed to examine the role of GMST in the fit to a GEV distribution (eq. 4) in this particular application, following CC2021. The value of α and its uncertainty range for the Siberian Heatwave do not seem to be explicitly discussed by CC2021. A linear regression of GMST anomalies against daily max temperatures gives a slope of 1.1 °C per °C (Fig. 3a), where the positive value indicates that the annual maximum daily temperatures at Verkhoyansk scale with GMST. The squared Pearson correlation, however, is only $r^2 = 0.01$, with a p-value of 0.2, indicating that GMST is only a weakly significant indicator of trends in Siberian temperature maxima.

Fig. 3b shows the maximum likelihood fit of a nonstationary GEV, including α , for multiple bootstrapping samples as specified in the Methods section. The estimate for the observations α without resampling in the observations is 1.8 °C per °C, similar to the slope of 1.1 obtained from the linear regression. The [2.5%, 97.5%] confidence interval is [-1.2, 4.8], while the 5% value is -0.7 (Fig. 3b; red plots). Both indicate that α is not significantly different from zero. While CC2021 did not provide an uncertainty range for α , they mention that the change in intensity of Siberian heatwaves (at a fixed probability) is estimated from their estimated PDF as 1.04 °C (with a 95% confidence interval from 0.35 to 3.4). There is no straightforward correspondence between this uncertainty range and that we calculate for α , unfortunately. We do note that the constraint that $|\xi| < 0.4$ imposed by CC2021 likely reduces their uncertainty range relative to the analysis we present here. The solution for all GEV parameters for the observations is given in Supplementary Fig. SI-2.

The deviance statistics, D , (section 2d) indicate that for the observations (Fig. 2b, leftmost bar), the addition of one more model parameter, α , representing the GMST dependence, is justified as the value is above the threshold indicated by the red horizontal line. Yet the deviance statistic uncertainty range includes a large range that is below the significance line, which seems appropriate given that the uncertainty range for α includes negative values.

To provide context for the interpretation of the observational results, we also examine output from the CESM Large Ensemble, which has time-varying anthropogenic forcing. We find that all ensemble members within the CESM Large Ensemble indicate a positive value of α , with a mean value of 2.60 °C per °C (Fig. 3b; blue plots). Similarly, 33 of 35 ensemble members give a deviance statistic that supports the use of a non-stationary component (that is, a GMST-dependence) in the GEV statistic (Fig. 2b).

The foremost reason that the Large Ensemble suggests a stronger link between Siberian extremes and GMST (that is, a larger α) may be that the LE, on average, simulates an Arctic-wide summer warming rate of 1.8 °C per °C warming in GMST, whereas an observational analysis only indicates a rate of 1.3 °C Arctic JJA warming per °C in GMST (using GISTEMP for both; Fig. 5a,b). One expects heatwaves to be strongly influenced by the JJA climatology, and Fig. 5c shows that different ensemble members, corresponding to different realizations of natural variability, show very different dependencies of the Arctic JJA climatology on GMST. It is difficult, therefore, to

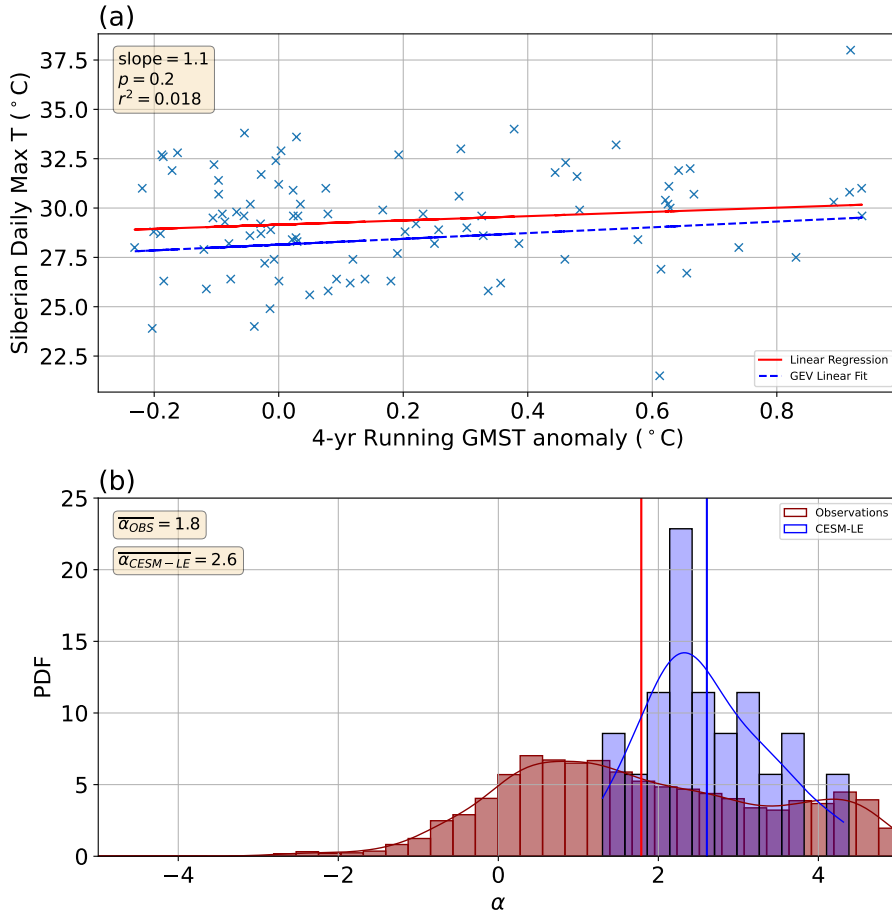


FIG. 3. **Siberian Heatwave: uncertainty in α .** (a) Scatter plot of the daily max temperature at the Verkhoyansk station against GMST. The red line indicates a linear regression fit to the data, and the blue line indicates a linear fit using the location parameter and α derived from the GEV maximum likelihood estimate. (b; red) PDF of the GEV-fit α distributions from the station data, using 5,000 bootstrap resamplings of the observed time series. The α value from the observations (no resampling) is shown by the vertical red line. (b; blue) Shown is a histogram of the GEV-fit α PDFs derived from the CESM Large Ensemble, where the α values are calculated from each ensemble member with no resampling. The average α value across the Large Ensemble is indicated with the blue line. There are 94 annual data points for each ensemble member.

estimate from the single realization corresponding to the observed record to what degree the Arctic JJA climatology is affected by anthropogenic climate change versus natural variability, adding to the uncertainty in attributing Siberian heatwaves. To address that, the WWA protocol includes

a step where the same analysis is applied to climate models, and results are reported from both sources.

Unsurprisingly, if data from multiple ensemble members are analyzed simultaneously as a single dataset, which mimics the availability of more data, the distribution of the GEV parameters narrows, generally converging around the mean value of the parameters across individual ensemble member fits (Fig. 4). The 95% confidence range for α (red asterisks in panel a) decreases from a large range of [1,4] ($^{\circ}\text{C per }^{\circ}\text{C}$) with one ensemble member to a smaller [2,3] range that may allow for a more reliable attribution with 10 ensemble members. Similar behavior is seen for the other GEV parameters. This implies that with a sufficiently long record, one can reduce the uncertainty in the GEV parameters, as expected, but that might require much more data than is expected to be available in the historical record anytime soon.

The overall result for the GMST dependence for the Siberian Heatwave analysis, which is the base of the attribution to anthropogenic climate change, seems superficially consistent with the results found from CC2021. However, the important caveats are that (1) we found in the previous subsection that internal variability can lead to GMST dependence that biases the value of α and hence the attribution results (Fig. 1a); (2) a GEV fit may, a priori, make sense to fit to annual daily temperature extremes being a block maxima time series. However, a normal distribution with $\alpha = 0$ does not appear to be ruled out for the observations (Fig. 2a). This may be a result of both the relatively short observational record and the autocorrelated nature of the temperature extremes which results in one year not being a sufficiently long block to justify a GEV fit. Still, a non-zero α is found to meaningfully improve the statistical fit to the CESM Large Ensemble Siberian extremes based on deviance statistics; (3) the uncertainty range for α , not explicitly mentioned in the original WWA analysis, includes negative values (Fig. 3b).

c. Australian Bushfire

We now consider the analysis of possible connections between the hot weather that may have contributed to the Australian Bushfires of the summer of 2020–2021 and anthropogenic climate change, using both observations and the CESM Large Ensemble, following the observational analysis of OK2021. We again find that a normal distribution and a GEV distribution (both with a constant mean/location parameter) fit the 7-day moving mean of daily temperature maxima in

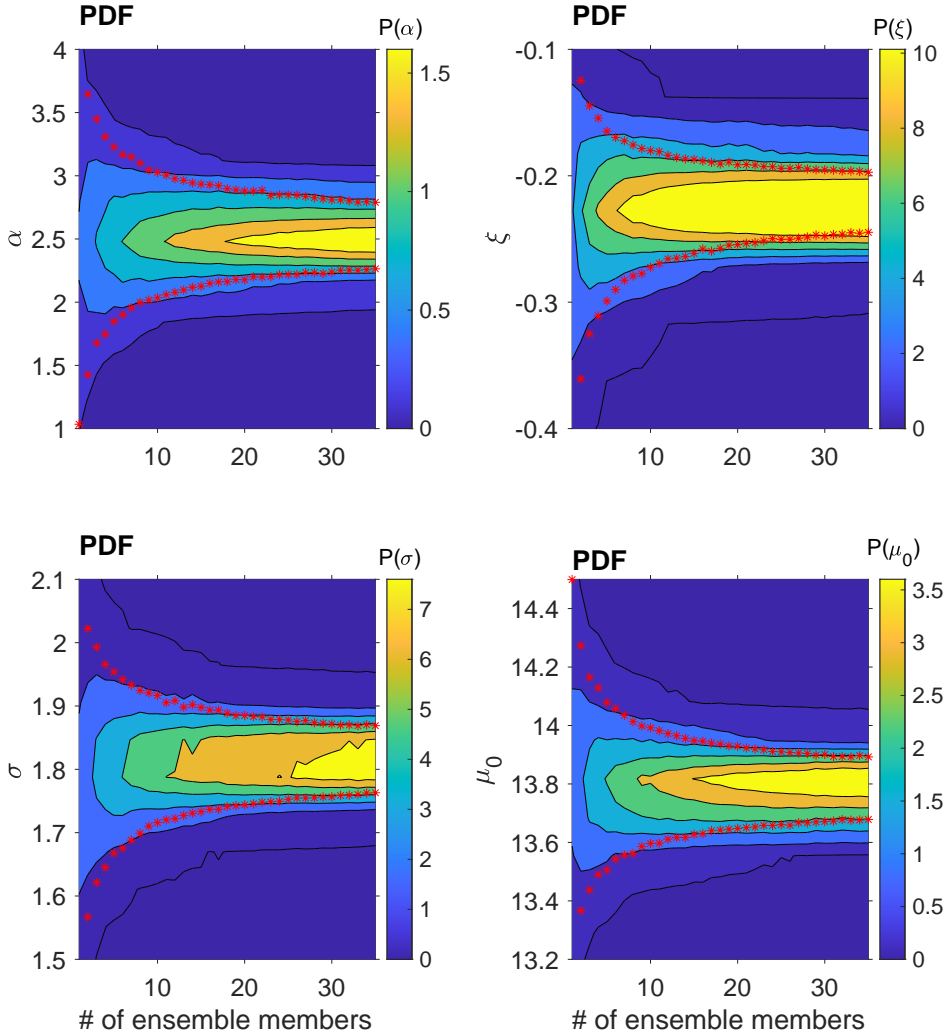


FIG. 4. **Siberian Heatwave: uncertainty in GEV parameters as a function of the number of ensemble members used.** Probability density function contour plots for each of the GEV parameters as a function of the number of ensemble members used from the CESM Large Ensemble and the parameter value. One ensemble member is equivalent in length to the historical record. Panel (a) represents the PDF for α , (b) ξ , (c) σ and (d) μ_0 . The PDFs were derived from the highest daily maximum Siberian temperature in June, as in CC2021, using the CESM Large Ensemble. Contours are drawn every 0.3 for (a), 2 for (b), 1.5 for (c), and 0.7 for (d), all starting at 0.05. We denote the 95% confidence range for each number of ensemble members by the red asterisks.

the observations without a GMST dependence well (Fig. 6a). In this case, a normal distribution fit to the empirical distribution has a mean absolute error (MAE) of 0.01, equal to the MAE for the GEV fit. Plots of the PDFs (Supplementary Fig. SI-3) for the three distributions (normal,

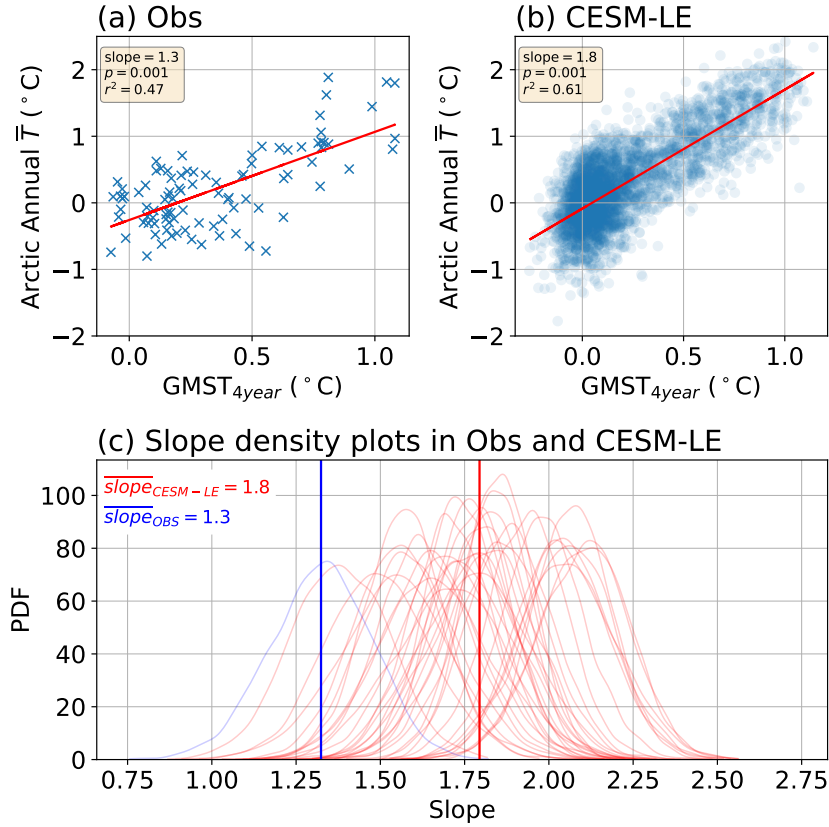


FIG. 5. **Natural variability and the attribution of Siberian heatwaves.** (a) A scatter plot of the annual average JJA Arctic (north of 70° N) surface temperatures against the 4-year running mean of GISTEMP annual GMST. (b) Same, for the 35 members of the CESM Large Ensemble over the period 1926–2019. (c) PDF of the slopes of annual average JJA Arctic surface temperatures against the 4-year running mean of annual GMST within each member of the CESM Large Ensemble with 5,000 bootstrap resamples (red). The same distribution is indicated for GISTEMP observations in blue. The vertical red line indicates the average slope across the CESM Large Ensemble, and the vertical blue line indicates the slope determined from observations.

GEV, and empirical) again suggest that the normal distribution aligns well with the observed data (to some degree due to the small number of data which does not constrain the PDF very well). Given that the normal distribution has one fewer parameter, it seems to offer a simpler approach to representing the data. The deviance statistic for the observations does suggest a significant GMST component (leftmost bar in Fig. 6b). However, given the possibility that this component is driven by natural variability rather than by anthropogenic change (section 3a, Fig. 1a), one must conclude again that even if α is justified statistically, it might represent the effects of natural variability rather

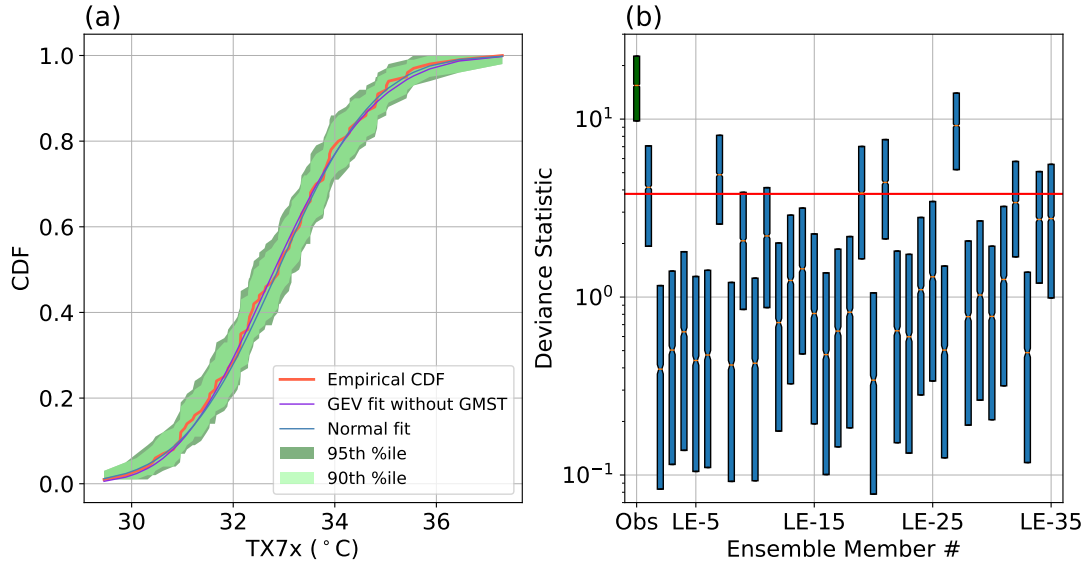


FIG. 6. **Australian Bushfire: (a) Testing the justification for a GEV.** The red curve indicates the empirical CDF of the highest annual 7-day running mean of daily maximum temperature over the area defined in van Oldenborgh et al. (2021) for observations. The purple and blue lines denote GEV (with a constant mean), and normal distribution fits, respectively. The light and dark green shadings correspond to 90th and 95th percentile confidence intervals. **(b) Justification for using a GMST-dependent mean.** Box plots of the deviance statistic between a GEV without a GMST component and a GEV with a GMST component using the Australia Bushfire example with 5,000 bootstrap resamples. The edges of the boxes correspond to the first and third quartiles. The deviance statistic was computed for each of the 35 members from the CESM Large Ensemble (blue) and compared with the 95th percentile significance level from a χ^2 distribution with one degree of freedom (red line). A box plot for the deviance statistic for observations is shown in green.

than anthropogenic climate change. In that case, it would be best not to use it for the purpose of attribution analysis, of course. The deviance statistic test for the CESM Large Ensemble shows that only five of the 35 ensemble members justify adding GMST dependence to the distribution parameters (Fig. 6b). This raises the question of whether the influence of GMST, and therefore of anthropogenic climate change in the WWA formulations, is a necessary part of the statistical description of extreme temperatures in Australia as represented in the CESM Large Ensemble.

The regression analysis of extreme temperatures and GMST, (Fig. 7a) as well as the range of α values estimated from observations (Fig. 7b; red) both show a GMST dependence near 2°C change in extreme temperatures per degree increase in GMST. As mentioned above, a sensible

null hypothesis for heatwaves in a warming climate is that the extreme values shift with the mean warming (Tziperman 2022). The GMST dependence calculated here suggests that Australian heatwaves increase at nearly twice the rate of the GMST. Such a strong response requires a physical mechanism. Some candidates are (1) the fact that land heats up more quickly than the ocean, so GMST always tends to lag behind land surface temperatures; (2) soil-drying can lead to further increases in warming over land as less water is available for evaporative cooling, etc. It is not clear that these can lead to a doubling of the GMST effect and further exploration of this is beyond the scope here. The alternative is that this is a result of natural variability (likely ENSO) affecting both Australian heat extremes and the GMST, consistent with Fig. 1a. Again, this suggests that using this value of α for attribution may lead to unreliable results. Finally, Fig. 7b (blue) shows a large range of GMST-dependencies for different ensemble members in the CESM Large Ensemble, again highlighting that a large component of this dependence most likely represents natural variability rather than anthropogenic change. The solution for all GEV parameters for the observations is given in Supplementary Fig. SI-4. How the GEV parameters scale with the number of CESM Large Ensemble members used is indicated in Supplementary Fig. SI-5.

d. Madagascar Drought

Finally, we consider the attribution analysis for the 2019–2021 drought in Madagascar, following the lead of HW2022. This case differs from the two examined above in that it analyzes precipitation extremes that are positive by definition. HW2022, therefore, used a different extreme value distribution function, the GPD, which is meant to represent the high tail of the distribution of extreme events over a specified threshold (Coles et al. 2001). As discussed in Section 2, HW2022 analyzed the driest 20% of the 2-year averages of precipitation data from 1951–2020 multiplied by minus one to turn minima (droughts) into maxima. We follow their example, with the important caveat made in Section 2b that the validity of using a GPD this way for precipitation data is not guaranteed given that there is a hard maximum of zero for these data of negative precipitation rates, a hard maximum that seems inconsistent with the definition of the GPD. We also note that taking the lowest 20% of 2-year precipitation data points amounts to only 14 data points, likely too low a number for a reliable attribution.

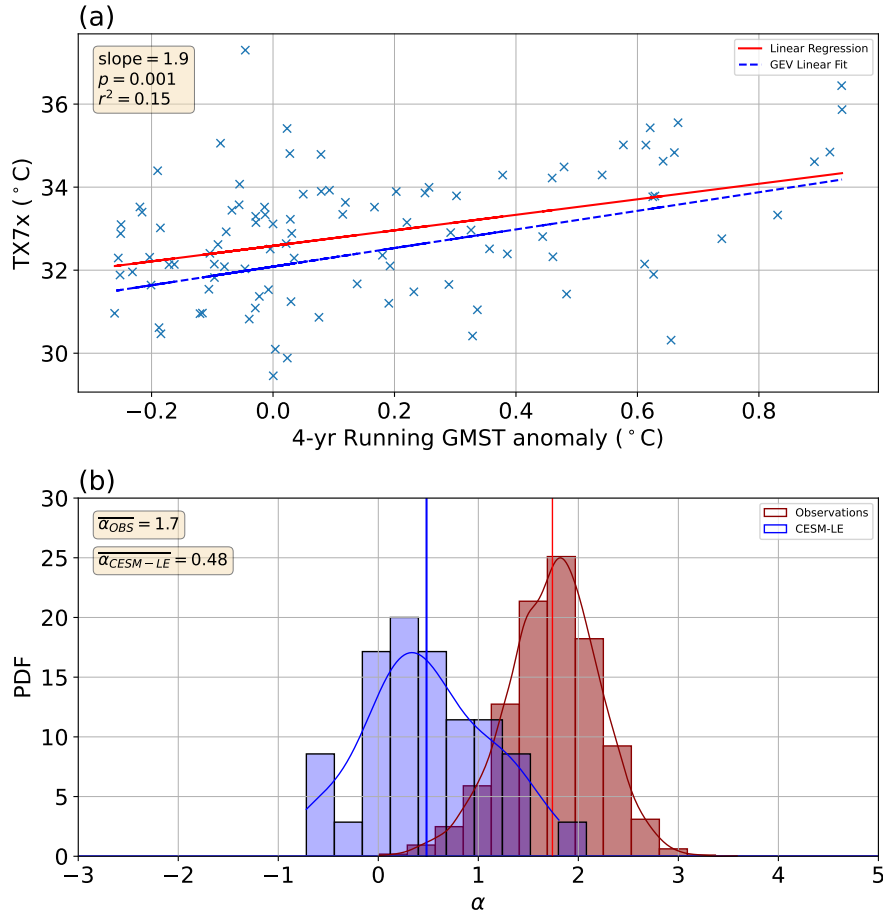


FIG. 7. **Australian Bushfire: distribution of α values.** (a) Scatter plot of the highest annual 7-day running mean of daily maximum temperatures against GMST (following van Oldenborgh et al. 2021). The red line indicates a linear regression fit to the data, and the blue line indicates a linear fit using the location parameter and α derived from the GEV maximum likelihood estimate. (b; red) PDF of the GEV-fit α distributions from observations, using bootstrap resampling. The α value from the observations without resampling is shown by the red line (at 1.7) (b; blue) Effect of the natural variability and number of data from a model large ensemble on the uncertainty in α for the Australian Bushfire example. Shown is a histogram of the GEV-fit α PDFs derived from the α value from each ensemble member with no resampling. The average α value across the Large Ensemble is indicated with the blue line.

Fig. 8d shows the MRL plot (section 2e) for the Madagascar Drought case. As a reminder, this plot needs to scale linearly within the range of the chosen threshold value for the GPD fit (section 2e) in order for the GPD analysis to be justified and self-consistent. For small and large

values of precipitation, the MRL curve appears to curve nonlinearly, indicating that a GPD fit is likely invalid using those thresholds. For precipitation thresholds ranging from roughly 1.6 to 2 mm/day, the MRL curve plateaus. The orange line shows the expected MRL line, $(\sigma + u\xi)/(1 - \xi)$; that slope does not align with the MRL curve around the value of 1.9 corresponding to the 20th percentile precipitation threshold chosen by Harrington et al. (2022). Likely the small number of data points is an obstacle for a reliable MRL plot here. In general, we suggest that this MRL analysis should be helpful in examining the self-consistency of applying a GPD to precipitation data. In this particular case it is not obvious if the required linear range exists in this plot to a degree that justifies using a GPD distribution and allows selecting a threshold.

We find again that an extreme value distribution is not required by the data distribution, and a GMST dependence is not needed: the GPD fit to the bottom 20th percentile precipitation data is no better than a log-normal distribution fitted to *all* of the precipitation data, both with constant distribution parameters that do not depend on the GMST (Fig. 8a). A log-normal distribution seems to be a reasonable null hypothesis for the positive precipitation data. In fact, the empirical CDF is practically unconstrained at its lower tail because there are no data points below a value of 1.25 mm/day.

The deviance statistic for the observations is marginally above the red significance line (leftmost green bar, Fig. 8b) suggesting that the inclusion of the additional model parameter α may be justified (uncertainty plots for the GPD parameters for observations are indicated in Supplementary Fig. SI-6). However, the bootstrap estimates for this parameter shown in Supplementary Fig. SI-7a show it to range over both negative and positive values, indicating that it cannot be calculated with any confidence. None of the 35 ensemble members exceed the deviance statistic significance level. It could be argued that Figure 1c, showing the analysis of the pre-industrial run, is evidence of the absence of any strong effect of natural variability modes on both GMST and Madagascar drought, in contrast with the analysis of Australian temperatures in Figure 1a. Also, Figure 8b may suggest that the CESM Large Ensemble does not adequately capture the effect of anthropogenic climate change on droughts in Madagascar.

As a reminder, the threshold parameter of the GPD, corresponding to the maximum precipitation value considered as an extreme drought year in this attribution case, was assumed by HW2022 to vary exponentially with the GMST (\bar{T}), as $\mu = \mu_0 \exp(\alpha \bar{T} / \mu_0)$ with $\mu_0 < 0$. If droughts become

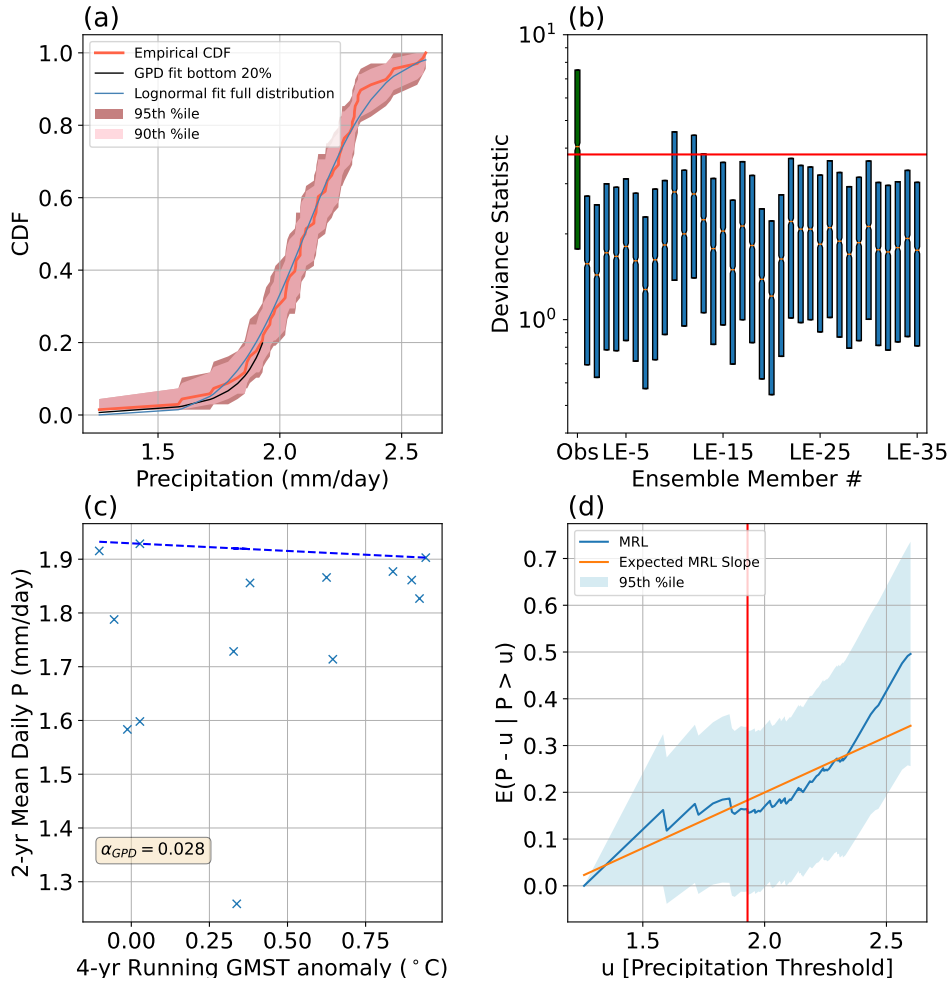


FIG. 8. **Madagascar Drought:** (a) Evaluating the need for a GPD fit. The empirical CDF is shown (red line, with 90th and 95th percentile confidence intervals shown by red shadings), based on 24-month running means of daily averaged annual precipitation over the Madagascar area defined in HW2022 using ERA5 precipitation. A GPD fit to the bottom 20th percentile precipitation (black) and a log-normal fit to the full distribution (blue). (b) The deviance statistic between a GPD with and without a GMST component in the CESM Large Ensemble (blue) and observations (green). (c) Scatter plot of the 2-year running mean of ERA5 daily precipitation over the Madagascar area defined in HW2022 against the 4-year running mean of annual GMST for the lowest 20 percent precipitation data. The dashed blue line shows the exponential GPD log-likelihood fit for the threshold parameter for the observations without resampling (eqn. 7) following HW2022. (d) MRL plot (section 2e) for different precipitation thresholds. The blue shading defines a region of confidence calculated as \pm one standard deviation. The red line denotes the threshold used in the GPD fit of HW2022 (i.e., the 20th percentile). The orange line represents the full linear equation from Equation 9 ($\sigma + u\xi/(1 - \xi)$).

more severe with increasing GMST, we expect the threshold parameter for the distribution of the negative precipitation to get larger (less negative) with increasing GMST, and therefore α/μ_0 to be negative and thus α to be positive. The value of α_{GPD} calculated from observations is small and indistinguishable from zero (Fig. 8c). The exponential fit was assumed by HW2022 in order to ensure that the scaling factor $\exp(\alpha\bar{T}/\mu_0)$ applied to both μ_0 and σ_0 is strictly positive, so the distribution has fixed dispersion (Philip et al. 2020). A scatter plot of ERA5 precipitation against GMST anomalies is shown in Fig. 8c. The dashed blue line indicated in the plot represents the exponential fit using the α and μ_0 coefficients from the maximum log-likelihood GPD fit. This fit looks notably linear, consistent with the Taylor expansion of the exponential function,

$$\mu = \mu_0 \exp(\alpha\bar{T}/\mu_0) \approx \mu_0(1 + \alpha\bar{T}/\mu_0) = \mu_0 + \alpha\bar{T}.$$

The small value of α found for observations indicates that the increase in GMST has had little effect on the statistics of two-year-average precipitation in Madagascar. Whereas this is also the conclusion reached by HW2022, we found that the data can be fitted with a log-normal distribution rather than GPD and without GMST dependence (Fig. 8a). Further, the deviance statistic only marginally justifies adding GMST dependence for observations and does not justify adding such dependence for model output (Fig. 8b). The fact that only 14 data points are involved in the fit seems much too small to draw any meaningful conclusions on an extreme value distribution as it leads to a large uncertainty interval shown by the shading. Supplemental Fig. SI-8a indicates that even if using the equivalent of 35 times as much data, the uncertainty range for α includes both positive and negative values. One could, therefore, conclude that the GPD approach is not likely to lead to confident attribution in this case in the next decades and beyond—even if there were actually an anthropogenic signal—given the small sample sizes from sub-sampling the bottom 20 percent of the precipitation data.

4. Conclusions

We were inspired in this work by a series of attribution studies by the “World Weather Attribution Project” (WWA) and evaluated the part of their methodology that involves a fit of observations to extreme value distribution functions. The full protocol used by this effort (Philip et al. 2020) uses additional tools and model analysis. The WWA method involves fitting an extreme value

distribution function to an observed record, with the distribution parameters depending on global mean surface temperature (GMST), whose variation is known to represent anthropogenic climate change. For example, the location parameter of an extreme value distribution (GEV) is made a linear function of GMST, \bar{T} , as $\mu = \mu_0 + \alpha \times \bar{T}$. The GMST dependence α is then used to calculate the change in return time of extreme events. This method was applied to many extreme events such as heatwaves, cold spells, floods, droughts, and more (e.g., van Oldenborgh et al. 2016; van der Wiel et al. 2017; van Oldenborgh et al. 2017; Ciavarella et al. 2021; van Oldenborgh et al. 2021; Harrington et al. 2022). We note that we are not the first study to scrutinize the WWA approach. García-Portela and Maraun (2023) discussed the WWA approach for CMIP model selection, i.e., that model spread should appropriately represent the full spread of dynamical aspects rather than subsetting to specific climate models that perform well on present-day climate. In our case, we examined the robustness of the results of three example WWA studies, demonstrated when they can fail due to the effects of natural variability, and suggested several additional statistical tests, reviewed below, that may increase confidence in the results of such an analysis.

We began by examining the GMST dependence of extreme heatwave events in Siberia (following CC2021), Australia (following OK2021), and drought in Madagascar (following OK2021), using data from a CESM preindustrial simulation. We found a significant GMST dependence in the first two cases, indicating that such dependence cannot be used to unequivocally identify the effects of anthropogenic climate change. The GMST dependence, in these cases, is a result of regional natural variability such as ENSO, which affects the extreme events being examined, and also weakly affects GMST. This seems to invalidate the use of a non-zero α to quantify the effect of anthropogenic climate change. The value of α in the Australian case is especially large, seemingly indicating that every degree increase in GMST leads to 5-degree increase in Australian heatwaves. Instead, we inferred that the large values of α are a result of natural variability (likely ENSO) affecting GMST by 0.2 degrees for every 1-degree effect it has on Australian heatwaves.

We tested if an extreme value distribution is indeed needed by plotting the empirical cumulative distribution function (CDF) with bootstrapping error bars (Figs. 2a, 6a, 8a). We found that fits using a standard distribution (normal or log-normal) fall within the error bars of the empirical distribution, indicating that there may not be a need for an extreme value distribution. Similarly, the standard distributions seem to fit the data well without a GMST dependence, indicating that

such dependence may not be justified by the data. We further tested if the addition of a GMST dependence of the distribution parameters is justified statistically using the log-likelihood ratio test, also known as the deviance statistics. When adding a parameter (specifically α), one expects the fit to improve, but the question is whether the improvement is beyond what is expected simply due to the addition of one more model parameter, so that one is convinced that the additional parameter represents a genuine effect in the data. We found that in the Australia and Madagascar cases, there is no justification for the addition of α .

The Madagascar drought attribution (HW2022) was based on only fourteen of the lowest two-year-averaged precipitation rates, hardly sufficient to construct a meaningful empirical CDF or to constrain the four parameters of the GPD distribution used for that purpose. In addition, computing two-year averages of precipitation and applying an extreme value distribution may lead to inconsistencies a priori given that averages converge to a Gaussian distribution (under the Central Limit Theorem). The GPD fit to the record, in this case, is meant for high values above a threshold, and the expected mean needs to vary linearly with the threshold chosen. We suggested that a mean residual life (MRL) plot can generally be used to test the self-consistency of using a GPD. In this case, it was not clear that these drought events are well represented by a GPD, but certainly, the number of data is insufficient for a meaningful MRL analysis in this particular case. To deal with the loss of data associated with this approach and difficulties in choice of the optimal precipitation threshold, Naveau et al. (2016) suggest instead using a statistical model fit to the full distribution of precipitation data, which has the added benefit of following the rules of extreme value theory for both high and low precipitation events. While our results—that attribution of two-year-averaged precipitation is not possible—agree with those of HW2022, we emphasized our different perspective that it is unlikely that attribution would be possible based on such a small number of data points, as well as the other difficulties pointed out above. In contrast, other approaches evaluating changes in the seasonal cycle of precipitation have led to the attribution of shifts in seasonal rainfall patterns in Southern Madagascar to climate change (Rigden et al. 2024).

An important issue raised by this work is the discrepancy between the modeled and observed findings, as seen, for example, in the deviance statistic results for the observations versus CESM Large Ensemble (Figs. 2b, 6b, 8b). This may be due to a particularly favorable sequence of internal variability in the observations, measurement error in the observational record, or issues with the

simulation of extreme weather in the CESM Large Ensemble. It would be helpful to test if these discrepancies also occur with other model large ensembles, including those used by WWA (Philip et al. (2020), OK2021).

Overall, our results suggest uncertainty in the interpretation of the dependence of the parameters of extreme event distributions on the global mean surface temperature as reflecting anthropogenic climate change. The proposed and demonstrated deviance statistic, MRL plot, and a careful analysis of uncertainty ranges, especially for α , may help avoid misguided confidence in attribution results. As noted in the introduction, WWA does not exclusively rely upon the empirical methodology evaluated here in order to reach conclusions, and also evaluates other historical data, model simulations, and the dynamical context. WWA also highlights some caveats associated with their study, including the necessity of testing for other probability laws (e.g., Gaussian, Gamma, etc.), covariates (ENSO, PDO, etc.), among others (Philip et al. 2020). Nevertheless, the WWA empirical methodology examined here still figures prominently in their analyses, and we have highlighted several caveats with its interpretation, foremost that internal variability can give rise to the appearance of strong covariance between GMST and local extremes. Our results do not provide evidence against a relationship between GMST and local extremes but, rather, that internal variability needs to be taken into account when fitting a distribution function to the record. As currently implemented, the WWA approach can lead to first-order biases in some cases. It, therefore, seems that it may be best to use the WWA empirical methodology in conjunction with other attribution approaches, which are summarized in the Introduction (e.g., Stott et al. 2016; Knutson et al. 2017; Seneviratne et al. 2021).

We suggest two key takeaways. First, controlling for internal variability, possibly by making the distribution parameters depend on additional covariates such as ENSO, appears important. This improvement upon the current method should be further developed. Second, empirical attribution techniques should be examined by applying the approach to simulations with and without changes to anthropogenic emissions. Application to such simulations will indicate whether the test is capable of discerning anthropogenic influences upon the statistics of extreme events. Although our focus is on the analysis of observation, some of our results are based on model output, and we use only one global climate model (CESM). This analysis should be extended to other climate models as well for purposes of further validation, although it seems that the main point of section a regarding the

interaction of natural variability and global mean surface temperature should be robust to model choice, at least qualitatively.

Acknowledgments. PS is supported by the Harvard Global Institute. ET is supported by DOE grant DE-SC0023134, and thanks the Weizmann Institute for its hospitality during parts of this work. PH is supported by NSF Award 2123295. The CESM project is supported primarily by the National Science Foundation (NSF). We acknowledge the CESM Large Ensemble Community Project and supercomputing resources provided by NSF/CISL/Yellowstone. We also acknowledge instructive conversations with Angela Rigden.

Data availability statement. All data used in this paper are available in public repositories. The climatological output from the CESM Large Ensemble and CESM preindustrial runs used in this paper are publicly available using the Intake-ESM Python package. All codes and data used here are available under the public open science foundation depository <https://osf.io/fycu2/>, DOI 10.17605/OSF.IO/FYCU2.

References

- Allen, M., 2003: Liability for climate change. *Nature*, **421 (6926)**, 891–892.
- Christidis, N., P. A. Stott, and F. W. Zwiers, 2015: Fast-track attribution assessments based on pre-computed estimates of changes in the odds of warm extremes. *Climate Dynamics*, **45 (5)**, 1547–1564.
- Ciavarella, A., and Coauthors, 2021: Prolonged Siberian heat of 2020 almost impossible without human influence. *Climatic Change*, **166 (1)**, 1–18.
- Clarke, B., F. Otto, R. Stuart-Smith, and L. Harrington, 2022: Extreme weather impacts of climate change: an attribution perspective. *Environmental Research: Climate*, **1 (1)**, 012 001.
- Coles, S., J. Bawa, L. Trenner, and P. Dorazio, 2001: *An introduction to statistical modeling of extreme values*, Vol. 208. Springer.
- Core Writing Team, H. Lee, and J. R. (eds.), 2023: Summary for Policymakers. *IPCC, 2023: Climate Change 2023: Synthesis Report. Contribution of Working Groups I, II and III to the Sixth Assessment Report of the Intergovernmental Panel on Climate Change*, Cambridge University Press, Cambridge, UK and New York, NY, USA, <https://doi.org/10.59327/IPCC/AR6-9789291691647.001>.
- De Paola, F., M. Giugni, F. Pugliese, A. Annis, and F. Nardi, 2018: Gev parameter estimation and stationary vs. non-stationary analysis of extreme rainfall in african test cities. *Hydrology*, **5 (2)**, <https://doi.org/10.3390/hydrology5020028>, URL <https://www.mdpi.com/2306-5338/5/2/28>.
- Faranda, D., S. Bourdin, M. Ginesta, M. Krouma, R. Noyelle, F. Pons, P. Yiou, and G. Messori, 2022: A climate-change attribution retrospective of some impactful weather extremes of 2021. *Weather and Climate Dynamics*, **3 (4)**, 1311–1340, <https://doi.org/10.5194/wcd-3-1311-2022>, URL <https://wcd.copernicus.org/articles/3/1311/2022/>.
- García-Portela, L., and D. Maraun, 2023: Overstating the effects of anthropogenic climate change? a critical assessment of attribution methods in climate science. *European Journal for Philosophy of Science*, **13 (1)**, 1–24.

- Gillett, N. P., and Coauthors, 2016: The detection and attribution model intercomparison project (damip v1. 0) contribution to cmip6. *Geoscientific Model Development*, **9** (10), 3685–3697.
- Harrington, L. J., and Coauthors, 2022: Limited role of climate change in extreme low rainfall associated with southern madagascar food insecurity, 2019–21. *Environmental Research: Climate*, **1** (2), 021 003, <https://doi.org/10.1088/2752-5295/aca695>, URL <https://dx.doi.org/10.1088/2752-5295/aca695>.
- Hegerl, G., and F. Zwiers, 2011: Use of models in detection and attribution of climate change. *Wiley interdisciplinary reviews: climate change*, **2** (4), 570–591.
- Hendon, H. H., D. W. Thompson, and M. C. Wheeler, 2007: Australian rainfall and surface temperature variations associated with the Southern Hemisphere annular mode. *Journal of Climate*, **20** (11), 2452–2467.
- Hersbach, H., and Coauthors, 2020: The era5 global reanalysis. *Quarterly Journal of the Royal Meteorological Society*, **146**, 1999 – 2049.
- Kay, J. E., and Coauthors, 2015: The Community Earth System Model (CESM) large ensemble project: A community resource for studying climate change in the presence of internal climate variability. *Bulletin of the American Meteorological Society*, **96** (8), 1333–1349.
- King, A. D., A. J. Pitman, B. J. Henley, A. M. Ukkola, and J. R. Brown, 2020: The role of climate variability in Australian drought. *Nature Climate Change*, **10** (3), 177–179.
- Knutson, T., J. Kossin, C. Mears, J. Perlwitz, and M. Wehner, 2017: Detection and attribution of climate change. *Climate Science Special Report: Fourth National Climate Assessment, Volume I*, U.S. Global Change Research Program, Washington, DC, USA.
- Lenssen, N., G. Schmidt, J. Hansen, M. Menne, A. Persin, R. Ruedy, and D. Zyss, 2019: Improvements in the gistemp uncertainty model. *J. Geophys. Res. Atmos.*, **124** (12), 6307–6326, <https://doi.org/10.1029/2018JD029522>.
- Lorenz, E. N., 1969: Atmospheric predictability as revealed by naturally occurring analogues. *Journal of Atmospheric Sciences*, **26** (4), 636–646.

Lott, F. C., N. Christidis, and P. A. Stott, 2013: Can the 2011 east african drought be attributed to human-induced climate change? *Geophysical Research Letters*, **40** (6), 1177–1181, <https://doi.org/https://doi.org/10.1002/grl.50235>, URL <https://agupubs.onlinelibrary.wiley.com/doi/abs/10.1002/grl.50235>.

National Academies of Sciences, 2016: *Attribution of extreme weather events in the context of climate change*. National Academies Press, Division on Earth and Life Studies and Board on Atmospheric Sciences and Committee on Extreme Weather Events and Climate Change Attribution.

Naveau, P., R. Huser, P. Ribereau, and A. Hannart, 2016: Modeling jointly low, moderate, and heavy rainfall intensities without a threshold selection. *Water Resources Research*, **52** (4), 2753–2769, <https://doi.org/https://doi.org/10.1002/2015WR018552>, URL <https://agupubs.onlinelibrary.wiley.com/doi/abs/10.1002/2015WR018552>, <https://agupubs.onlinelibrary.wiley.com/doi/pdf/10.1002/2015WR018552>.

Otto, F. E., S. Philip, S. Kew, S. Li, A. King, and H. Cullen, 2018: Attributing high-impact extreme events across timescales—a case study of four different types of events. *Climatic change*, **149**, 399–412.

Otto, F. E. L., and Coauthors, 2020: Challenges to understanding extreme weather changes in lower income countries. *Bulletin of the American Meteorological Society*, **101** (10), E1851 – E1860, <https://doi.org/10.1175/BAMS-D-19-0317.1>, URL <https://journals.ametsoc.org/view/journals/bams/101/10/bamsD190317.xml>.

Pascale, S., S. B. Kapnick, T. L. Delworth, and W. F. Cooke, 2020: Increasing risk of another cape town "day zero" drought in the 21st century. *Proceedings of the National Academy of Sciences*, **117** (47), 29 495–29 503.

Pendergrass, A. G., 2018: What precipitation is extreme? *Science*, **360** (6393), 1072–1073, <https://doi.org/10.1126/science.aat1871>, URL <https://www.science.org/doi/abs/10.1126/science.aat1871>, <https://www.science.org/doi/pdf/10.1126/science.aat1871>.

- Perkins, S., A. Pitman, N. J. Holbrook, and J. McAneney, 2007: Evaluation of the ar4 climate models' simulated daily maximum temperature, minimum temperature, and precipitation over australia using probability density functions. *Journal of climate*, **20** (17), 4356–4376.
- Philip, S., and Coauthors, 2020: A protocol for probabilistic extreme event attribution analyses. *Advances in Statistical Climatology, Meteorology and Oceanography*, **6** (2), 177–203.
- Pinto, I., R. Barimalala, S. Philip, M. Zachariah, S. Sengupta, and M. Vahlberg, 2023: Extreme poverty rendering madagascar highly vulnerable to underreported extreme heat that would not have occurred without human-induced climate change. Tech. rep., Grantham Institute-Climate Change and the Environment.
- Rigden, A., C. Golden, D. Chan, and P. Huybers, 2024: Climate change linked to drought in southern madagascar. *npj Climate and Atmospheric Science*, **7** (1), 1–9.
- Robin, Y., and A. Ribes, 2020: Nonstationary extreme value analysis for event attribution combining climate models and observations. *Advances in Statistical Climatology, Meteorology and Oceanography*, **6** (2), 205–221, <https://doi.org/10.5194/ascmo-6-205-2020>, URL <https://ascmo.copernicus.org/articles/6/205/2020/>.
- Seneviratne, S., and Coauthors, 2021: Weather and climate extreme events in a changing climate. *Climate Change 2021: The Physical Science Basis. Contribution of Working Group I to the Sixth Assessment Report of the Intergovernmental Panel on Climate Change*, Cambridge University Press, Cambridge, United Kingdom and New York, NY, USA.
- Stott, P. A., N. P. Gillett, G. C. Hegerl, D. J. Karoly, D. A. Stone, X. Zhang, and F. Zwiers, 2010: Detection and attribution of climate change: a regional perspective. *Wiley interdisciplinary reviews: climate change*, **1** (2), 192–211.
- Stott, P. A., D. Stone, and M. R. Allen, 2004: Human contribution to the european heatwave of 2003. *Nature*, **432** (7017), 610–614.
- Stott, P. A., and Coauthors, 2016: Attribution of extreme weather and climate-related events. *WIREs Climate Change*, **7** (1), 23–41, <https://doi.org/https://doi.org/10.1002/wcc.380>, URL <https://wires.onlinelibrary.wiley.com/doi/abs/10.1002/wcc.380>, <https://wires.onlinelibrary.wiley.com/doi/pdf/10.1002/wcc.380>.

- Trevino, A. M., K. A. McKinnon, and P. J. Huybers, 2020: Extremely wrong: When limited data leads to biases in general extreme values distribution estimates. *AGU Fall Meeting Abstracts*, Vol. 2020, A147–0010.
- Tziperman, E., 2022: *Global Warming Science: A Quantitative Introduction to Climate Change and Its Consequences*. Princeton University Press, 336 pp.
- Ummenhofer, C. C., M. H. England, P. C. McIntosh, G. A. Meyers, M. J. Pook, J. S. Risbey, A. S. Gupta, and A. S. Taschetto, 2009: What causes southeast Australia’s worst droughts? *Geophysical Research Letters*, **36** (4).
- van der Wiel, K., and Coauthors, 2017: Rapid attribution of the august 2016 flood-inducing extreme precipitation in south louisiana to climate change. *Hydrology and Earth System Sciences*, **21** (2), 897–921, <https://doi.org/10.5194/hess-21-897-2017>, URL <https://hess.copernicus.org/articles/21/897/2017/>.
- van Oldenborgh, G. J., F. E. L. Otto, K. Haustein, and K. AchutaRao, 2016: The heavy precipitation event of december 2015 in chennai, india. *Bulletin of the American Meteorological Society*, **97** (12), S87 – S91, <https://doi.org/10.1175/BAMS-D-16-0129.1>, URL <https://journals.ametsoc.org/view/journals/bams/97/12/bams-d-16-0129.1.xml>.
- Van Oldenborgh, G. J., A. Van Urk, and M. Allen, 2012: The absence of a role of climate change in the 2011 thailand floods. *Bull. Amer. Meteor. Soc.*, **93**, 1047–1049.
- van Oldenborgh, G. J., and Coauthors, 2017: Attribution of extreme rainfall from hurricane harvey, august 2017. *Environmental Research Letters*, **12** (12), 124 009, <https://doi.org/10.1088/1748-9326/aa9ef2>, URL <https://dx.doi.org/10.1088/1748-9326/aa9ef2>.
- van Oldenborgh, G. J., and Coauthors, 2021: Attribution of the Australian bushfire risk to anthropogenic climate change. *Natural Hazards and Earth System Sciences*, **21** (3), 941–960.
- Vautard, R., and P. Yiou, 2009: Control of recent european surface climate change by atmospheric flow. *Geophysical Research Letters*, **36** (22).
- Yamaguchi, M., J. C. Chan, I.-J. Moon, K. Yoshida, and R. Mizuta, 2020: Global warming changes tropical cyclone translation speed. *Nature Communications*, **11** (47).

Yiou, P., R. Vautard, P. Naveau, and C. Cassou, 2007: Inconsistency between atmospheric dynamics and temperatures during the exceptional 2006/2007 fall/winter and recent warming in Europe. *Geophysical Research Letters*, **34** (21).

Yoshida, K., M. Sugi, R. Mizuta, H. Murakami, and M. Ishii, 2017: Future changes in tropical cyclone activity in high-resolution large-ensemble simulations. *Geophysical Research Letters*, **44** (19), 9910–9917, <https://doi.org/10.1002/2017GL075058>, URL <https://agupubs.onlinelibrary.wiley.com/doi/abs/10.1002/2017GL075058>.

Zwiers, F. W., X. Zhang, and Y. Feng, 2011: Anthropogenic influence on long return period daily temperature extremes at regional scales. *Journal of Climate*, **24** (3), 881 – 892, <https://doi.org/10.1175/2010JCLI3908.1>, URL <https://journals.ametsoc.org/view/journals/clim/24/3/2010jcli3908.1.xml>.

Supplementary material

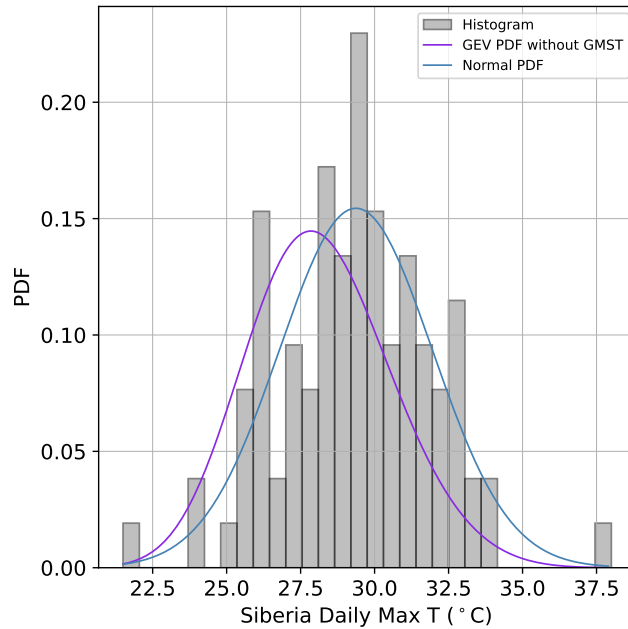


FIG. SI-1. **PDF comparisons.** The histogram shows the highest daily maximum temperature for each year for the Verkhoyansk station data. The purple and blue lines denote PDF fits by a GEV (with a constant location parameter) and by a normal distribution, respectively.

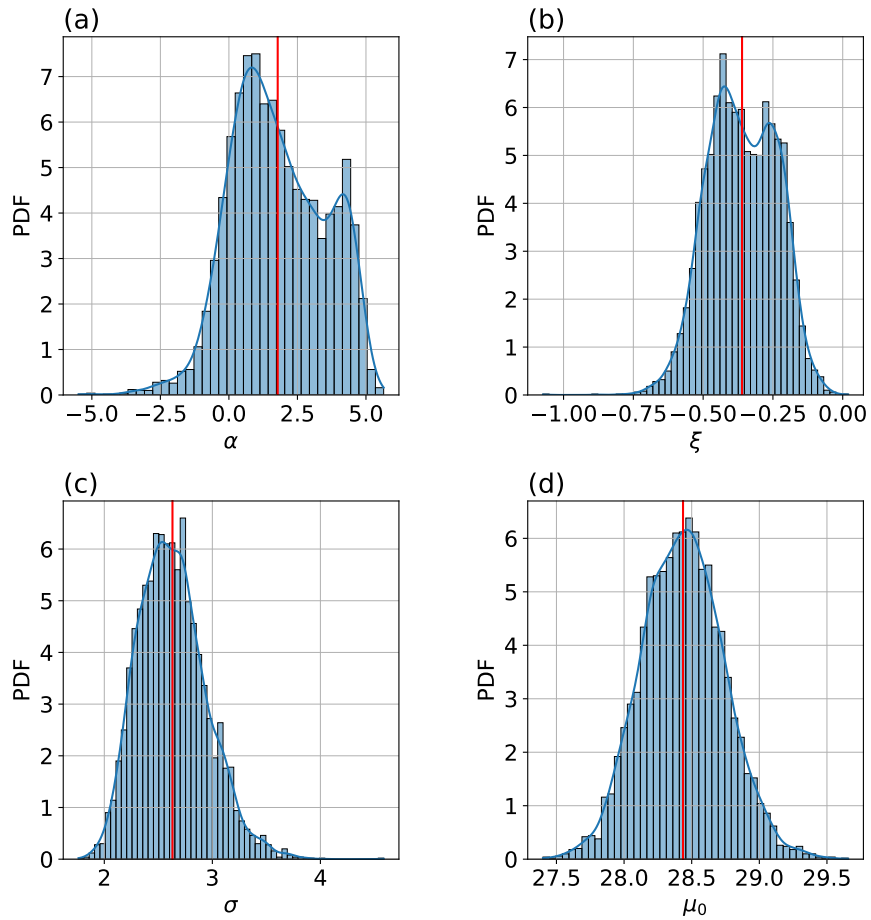


FIG. SI-2. **Siberian Heatwave: distribution of observation GEV values.** Probability distribution functions of the GEV parameters using a 5,000-times bootstrap resampling of the annual observational time series.

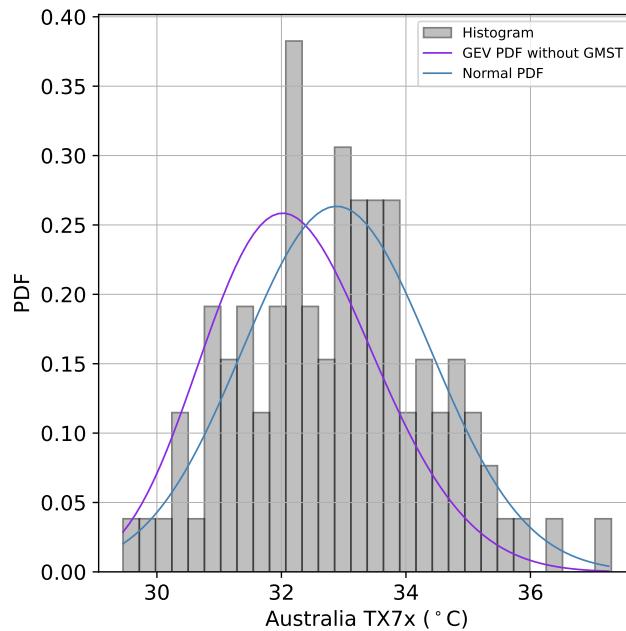


FIG. SI-3. **PDF comparisons.** The histogram shows the annual (July–June) maxima of 7-day moving average daily-maximum surface temperature over the area defined in van Oldenborgh et al. (2021). The purple and blue lines denote PDF fits by a GEV (with a constant location parameter) and by a normal distribution, respectively.

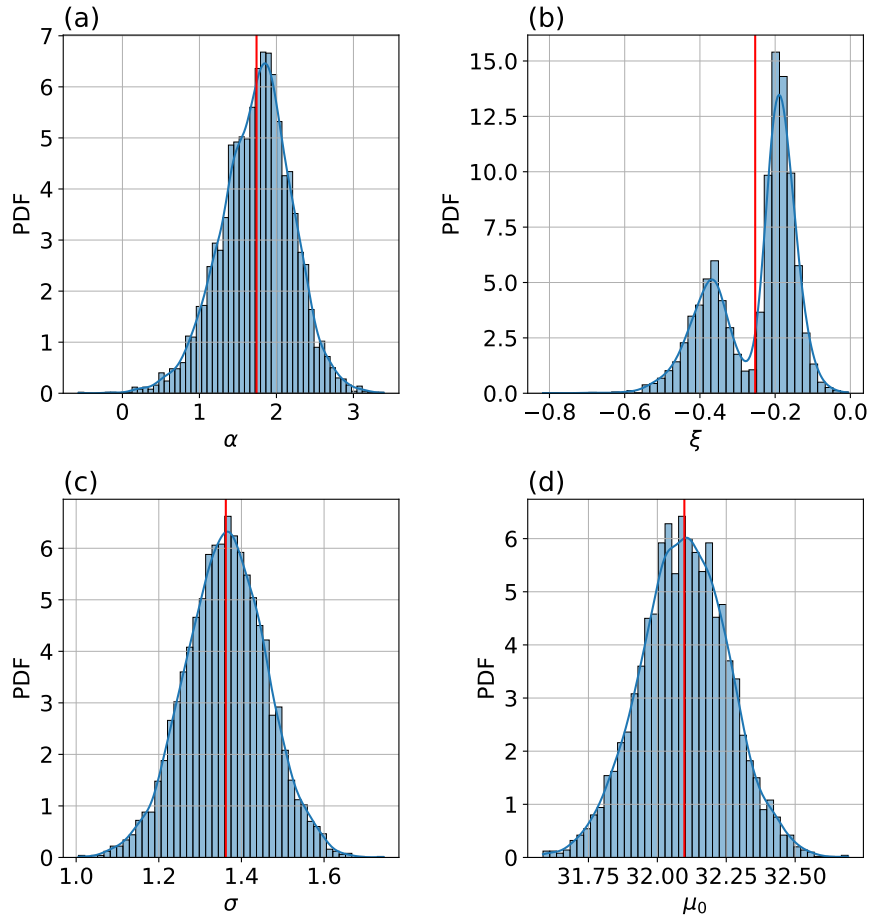


FIG. SI-4. **Australia Bushfire: distribution of GEV parameter values calculated for the observed record.** Probability distribution functions of the GEV parameters using a 5,000-times bootstrap resampling of the observed annual time series. The mean values for each parameter are indicated with the red lines within each panel. The double peak structure of the ξ distribution is purely a result of one data point seen as the highest 7-day running mean of daily maximum temperatures at GMST ≈ 0 in Fig. 7a. Removing that data point leads to a single peak ξ distribution connecting the two peaks seen here. The distributions of the other GEV parameters are not significantly affected by the removal of that data point.

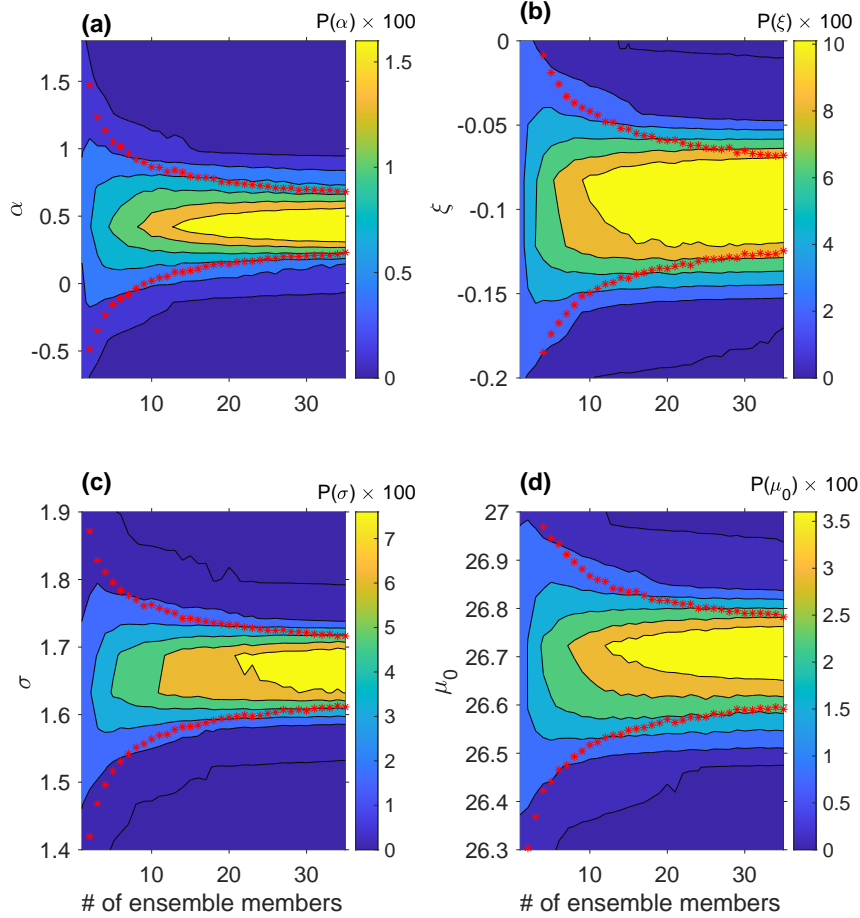


FIG. SI-5. **Australian Bushfire: dependence of confidence in GEV parameters on the number of ensemble members.** Probability distribution functions of the GEV parameters as a function of the number of ensemble members used. The data were derived from the highest annual 7-day running mean of daily maximum temperatures, as in van Oldenborgh et al. (2021), but using the CESM Large Ensemble. Smaller values over a column indicate a greater spread in the distribution of the parameter. Contour levels are indicated every 0.3 for (a), 2 for (b), 1.5 for (c), and 0.7 for (d), all starting at 0.1. We denote the 95% confidence range for each number of ensemble members by the red asterisks.

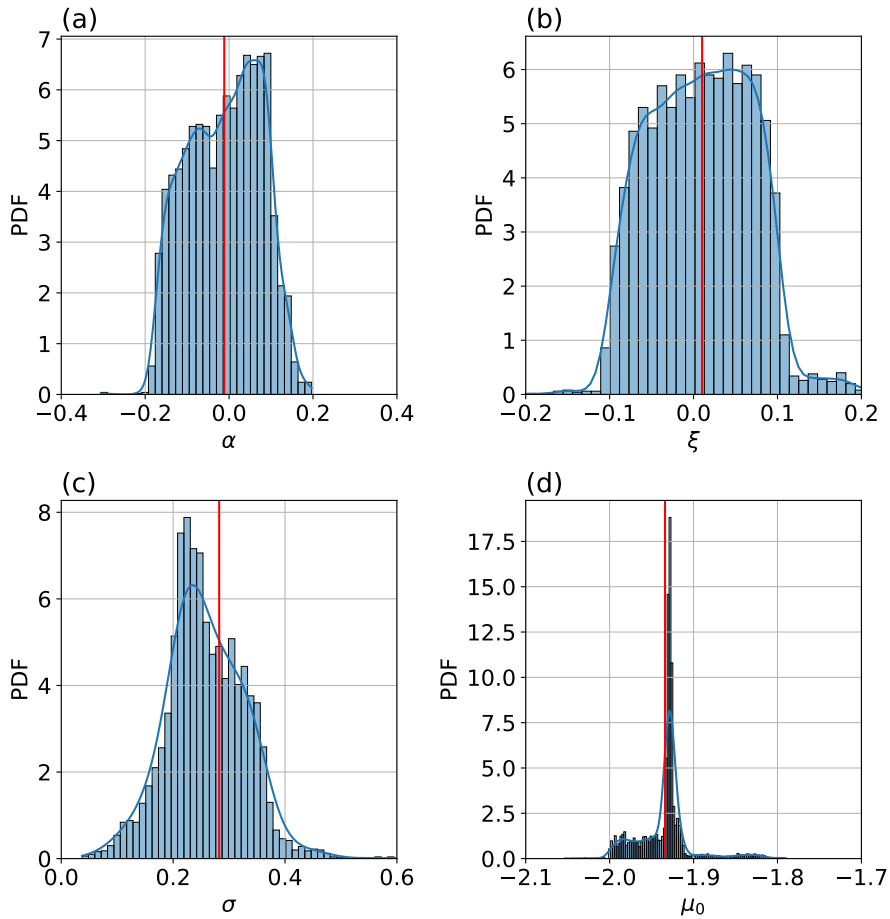


FIG. SI-6. **Madagascar Drought: distribution of observation GPD values.** Probability distribution functions of the GPD parameters using a 5,000-times bootstrap resampling of the annual observational time series. The mean values for each parameter are indicated with the red lines within each panel.

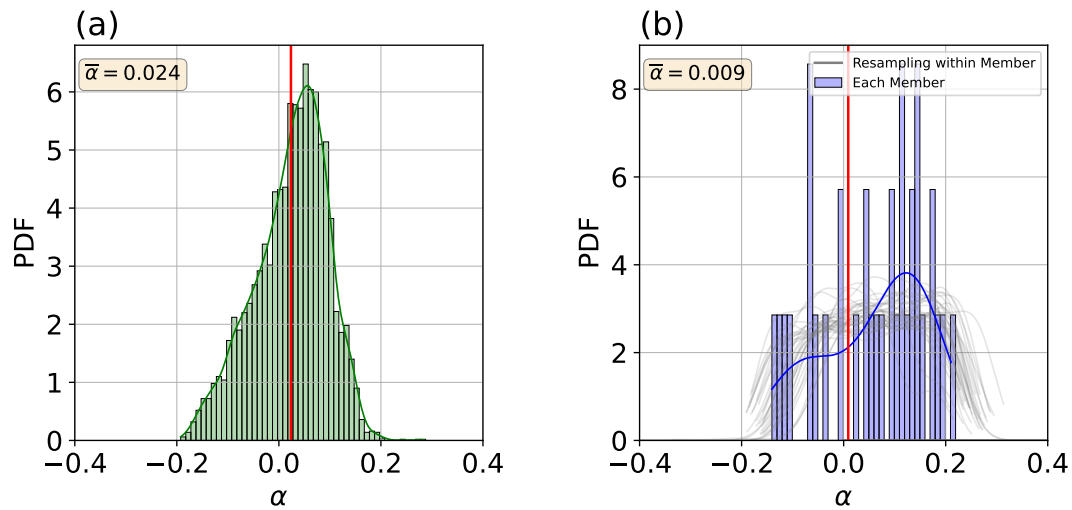


FIG. SI-7. **Madagascar Drought: distribution of α values.** (a) PDF of the GEV-fit α distributions from observations, using bootstrap resampling. The mean α value for the observations is indicated with the red line (at 0.026). (b) Effect of the number of data on the uncertainty in α for the Madagascar Drought example. Shown is a histogram of the GEV-fit α PDFs derived from the α value from each ensemble member with no resampling (blue). The resampling of the data within each ensemble member is indicated with the gray curves.

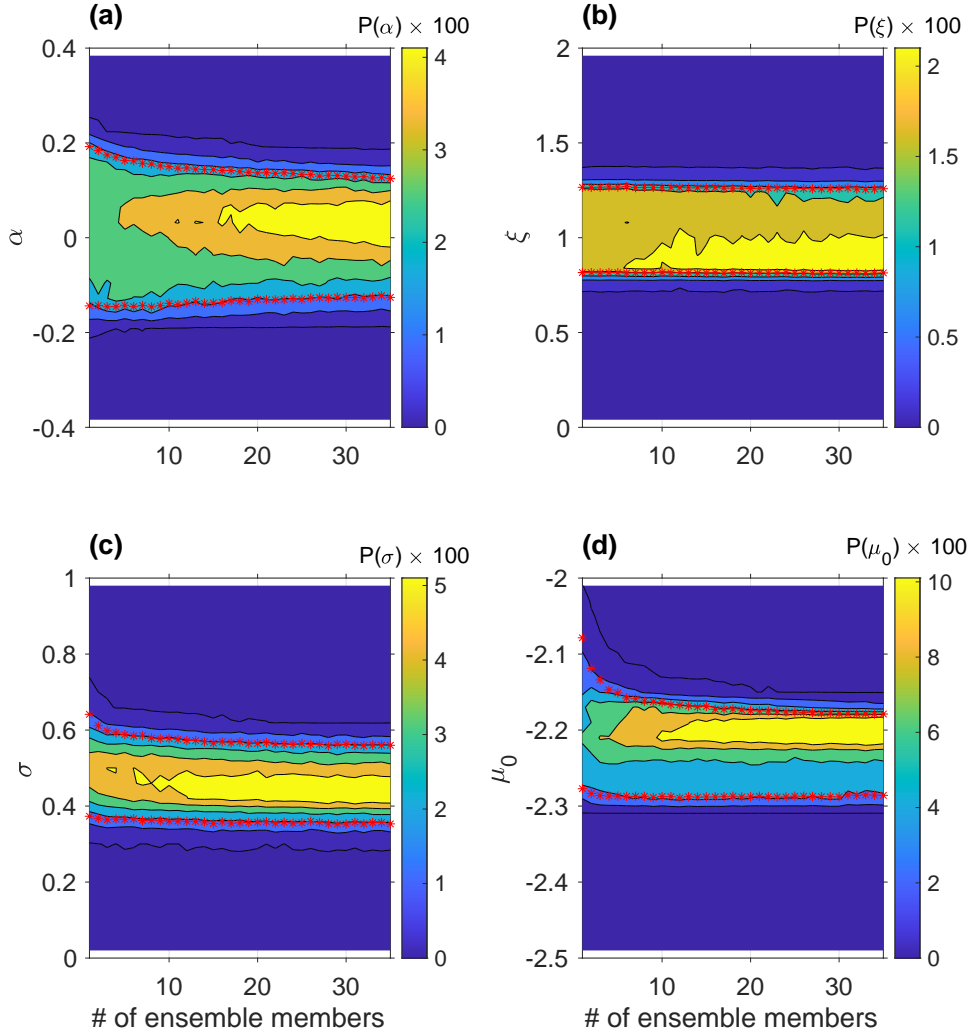


FIG. SI-8. **Madagascar Drought: dependence of confidence in GPD parameters on the number of ensemble members.** Probability distribution functions of the GPD parameters as a function of the number of ensemble members used. Contour levels are indicated every 0.8 for (a), 0.4 for (b), 1 for (c), and 2 for (d), all starting at 0.1. We denote the 95% confidence range for each number of ensemble members by the red asterisks.